



1 **The seismo-hydro-mechanical behaviour during deep geothermal**
2 **reservoir stimulations: open questions tackled in a decameter-**
3 **scale in-situ stimulation experiment**

4 Amann Florian¹, Valentin Gischig¹, Keith Evans¹, Joseph Doetsch¹, Reza Jalali¹, Benoît
5 Valley², Hannes Krietsch¹, Nathan Dutler², Linus Villiger¹, Bernard Brixel¹, Maria
6 Klepikova¹, Anniina Kittilä¹, Claudio Madonna¹, Stefan Wiemer¹, Martin O. Saar¹, Simon
7 Loew¹, Thomas Driesner¹, Hansruedi Maurer¹, Domenico Giardini¹,

8

9 ¹ETH Zurich, Department of Earth Sciences, Sonneggstrasse 5, 8092 Zurich, Switzerland

10 ²University of Neuchâtel, Centre for Hydrogeology and Geothermics (CHYN), Laboratory of
11 Geothermics and Reservoir Geomechanics, 2000 Neuchâtel, Switzerland

12

13

14

15

16

17

18

19

20

21

22

23 **Keywords:** Deep geothermal energy, EGS, induced seismicity, in-situ experiments, hydro-
24 mechanical coupled processes in EGS,



25 **Abstract**

26 In this contribution we present a review of scientific research results that address seismo-
27 hydro-mechanical coupled processes relevant for the development of a sustainable heat
28 exchanger in low permeability crystalline rock and introduce the design of the In-situ
29 Stimulation and Circulation (ISC) experiment at the Grimsel Test Site dedicated to study such
30 processes under controlled conditions. The review shows that research on reservoir
31 stimulation for deep geothermal energy exploitation has been largely based on laboratory
32 observations, large-scale projects and numerical models. Observations of full-scale reservoir
33 stimulations have yielded important results. However, the limited access to the reservoir and
34 limitations in the control on the experimental conditions during deep reservoir stimulations is
35 insufficient to resolve the details of the hydro-mechanical processes that would enhance
36 process understanding in a way that aids future stimulation design. Small scale laboratory
37 experiments provide a fundamental insights into various processes relevant for enhanced
38 geothermal energy, but suffer from 1) difficulties and uncertainties in upscaling the results to
39 the field-scale and 2) relatively homogeneous material and stress conditions that lead to an
40 over-simplistic fracture flow and/or hydraulic fracture propagation behaviour that is not
41 representative for a heterogeneous reservoir. Thus, there is a need for intermediate-scale
42 hydraulic stimulation experiments with high experimental control that bridge the various
43 scales, and for which access to the target rock mass with a comprehensive monitoring system
44 is possible. Only few intermediate-scale hydro-shearing and hydro-fracturing experiments
45 have recently been performed in a densely instrumented rock mass. No such measurements
46 have been performed on faults in crystalline basement rocks. The In-situ Stimulation and
47 Circulation (ISC) experiment currently performed in a naturally fractured and faulted
48 crystalline rock mass at the Grimsel Test Site (Switzerland) is designed to address open
49 research questions, which could not be investigated in the required detail so far. Two
50 hydraulic injection phases were executed to enhance the permeability of the rock mass: a
51 hydro-shearing phase and then a hydraulic fracturing phase. During the injection phases the
52 rock mass deformation across fractures and within intact rock, the pore pressure distribution
53 and propagation and the micro-seismic response were monitored at a high spatial and
54 temporal resolution.

55



56 1 Introduction

57 The necessity to produce carbon dioxide neutral electricity, ideally as base-load power (i.e. 24
58 hours a day, year-round) and the increased aversion to nuclear power generation have
59 motivated global efforts to optimize methods for extracting deep geothermal energy for
60 electricity production. However, currently, geothermal power production is limited to distinct
61 geological conditions, where fluid flow rate in geothermal reservoirs carry sufficient heat
62 (Saar, 2011) and/or pressure for economic power generation (Randolph and Saar, 2011a;
63 Breede et al., 2013; Adams et al., 2015). It is widely agreed that the earth's crust holds
64 substantially more geothermal resources than are presently being exploited (e.g. Tester et al.,
65 2006). However, standard water- or brine-based geothermal power generation requires
66 persistent high reservoir permeabilities of at least 10^{-16} m² (Manning and Ingebritsen, 1999)
67 and temperatures of ideally over about 170°C (e.g., Evans, 2014; Saar, to be published in
68 2017), as otherwise it is not economic. When such temperatures are not present at relatively
69 shallow depths of a couple of kilometres, unconventional geothermal methods need to be
70 employed. One such approach targets formation temperatures of approximately 170-200°C in
71 regions with standard geothermal gradients of about 30°C/km, thus requiring wells to be
72 drilled to at least 5 to 6 km depth into crystalline hard rock. The two main difficulties of
73 implementing these so-called Enhanced or Engineered Geothermal Systems (EGS), originally
74 termed Hot Dry Rock (HDR) systems (Brown et al., 2012), are that 1) rotary drilling to such
75 depths is presently uneconomic on a routine basis and 2) permeabilities of hard rocks at those
76 depths are typically too low (e.g., Manning and Ingebritsen, 1999; Saar and Manga, 2004) to
77 enable circulation of fluids to advectively extract the heat (and pressure) energy
78 economically. Consequently, EGS virtually always require hydraulic stimulation to enhance
79 the permeability to such a degree that economic geothermal power generation becomes
80 possible. However, the goal of sufficiently enhancing permeability has not yet been achieved
81 in a sustained way, despite attempts since the 1970s (Evans, 2014). Additionally, induced
82 seismicity is a common problem with EGS (e.g., Giardini, 2009).

83 In this contribution, we focus on how a subsurface heat exchanger may be constructed
84 between boreholes at depth within low-permeability rock to form EGS, where a fluid,
85 typically water or brine, may then be circulated more easily than before. The artificially
86 enhanced permeability needs to be high enough to reach flow rates that are commercially
87 relevant for power production, depending on the subsurface working fluid. Larger
88 permeability enhancements are required for water or brine than for CO₂, as the latter can
89 utilize lower temperatures and lower permeabilities for economic geothermal power



90 generation, due to its higher energy conversion efficiency (Brown, 2000; Pruess, 2006, 2007;
91 Randolph and Saar, 2011a, 2011b; Adams et al., 2014, 2015; Garapati et al., 2015; Buscheck,
92 2016). Moreover, fluid flow should occur within a large number of permeable fracture
93 pathways that sweep a large surface area of the rock, thereby providing longevity to the
94 system and avoiding early thermal breakthrough, such as occurred at the Rosemanowes
95 Project (Parker, 1999) and the Hijiori Project (Tenma et al., 2008). The construction of such
96 systems (i.e. an artificial reservoir with sufficient permeability for energy extraction) is one of
97 the key research challenges for unlocking the large potential of deep geothermal energy. The
98 creation of a subsurface heat-exchanger between the boreholes in the low permeability rock
99 mass typically involves hydraulic stimulation, i.e. fluid injections, during which the pore
100 pressure is raised in the rock mass leading to the enhancements of permeability of natural
101 fractures and faults, and perhaps the creation of new fractures.

102 Hydraulic stimulation is inevitably accompanied by induced seismicity (e.g., Zoback and
103 Harjes, 1997; Evans et al., 2005a; Davis et al., 2013, Bao and Eaton, 2016), because the slip
104 triggered by the elevated pore pressure arising from injections may be sufficiently rapid to
105 generate seismic waves. In shale gas- and EGS-related stimulations, clouds of induced
106 seismic events are important monitoring tools for delineating the location, where rock mass
107 volume is undergoing stimulation (e.g., Wohlhard et al., 2006). Unfortunately, seismic events
108 induced by the stimulation injections may be large enough to be felt by local populations and
109 even to cause infrastructure damage (e.g., in Basel, 2006; Giardini, 2009). In the past few
110 years, induced seismicity has been recognized as a significant challenge to the widespread
111 deployment of EGS technology. From a reservoir engineering perspective, EGS faces two
112 competing but interrelated issues: 1) rock mass permeability must be significantly enhanced
113 by several orders of magnitude within a sufficiently large volume to enable sustainable heat
114 extraction over many years (i.e., 20 – 30 years) while 2) keeping the associated induced
115 seismicity below a hazardous level (Evans et al. 2014). Designing reservoir stimulation
116 practices that optimize permeability creation and minimize induced seismicity requires a
117 greatly improved understanding of the seismo-hydro-mechanical (SHM) response of the
118 target rock mass volume. Seismo-hydro-mechanical processes relevant for stimulation
119 involve 1) HM-coupled fluid flow and pressure propagation, 2) transient pressure- and
120 permanent slip-dependent permeability changes, 3) fracture formation and interaction with
121 pre-existing structures, 4) rock mass deformation around the stimulated volume due to fault
122 slip, failure processes and poroelastic effects, and 5) the transition from aseismic to seismic
123 slip.



124 A decameter-scale, in-situ, stimulation and circulation (ISC) experiment is currently being
125 conducted at the Grimsel Test Site (GTS) in Switzerland with the objective of improving our
126 understanding of the aforementioned HM-coupled processes in a moderately fractured
127 crystalline rock mass. The ISC experiment activities aim to support the development of EGS
128 technology by 1) advancing the understanding of fundamental processes that occur within the
129 rock mass in response to relatively large-volume fluid injections at high pressures, 2)
130 improving the ability to estimate and model induced seismic hazard and risk, 3) assessing the
131 potential of different injection protocols to keep seismic event magnitudes below an
132 acceptable threshold, 4) developing novel monitoring and imaging techniques for pressure,
133 temperature, stress, strain and displacement as well as geophysical methods such as ground-
134 penetrating radar (GPR), passive and active seismics and 5) generating a high-quality
135 benchmark dataset that facilitates the development and validation of numerical modelling
136 tools.

137 This paper presents a literature review that highlights key research gaps concerning hydraulic
138 reservoir stimulation, and discusses which of the aforementioned research questions can be
139 addressed in our decameter underground stimulation experiment. We then provide an
140 overview of the ISC project that describes the geological site conditions, the different project
141 phases and the monitoring program.

142

143 2 Literature review

144 2.1 Stimulation process

145 The concept of mining heat from hot, low permeability rock at great depth was first proposed
146 at Los Alamos National Labs in the 1970s and was called Hot Dry Rock system (Brown et al.,
147 2012). They initially envisaged creating a reservoir by applying oil and gas reservoir
148 hydrofracture technology to build a heat exchanger between two boreholes. Subsequent field
149 tests have demonstrated that hydraulic stimulation injections are effective in enhancing the
150 permeability of a rock mass by several orders of magnitude by producing irreversible fracture
151 opening, whilst also increasing the connectivity of the fracture network (Kaieda et al., 2005,
152 Evans et al., 2005b; Häring et al., 2008). Two different 'end-member' mechanisms commonly
153 appear in discussions of permeability creation processes through hydraulic injections: 1)
154 hydraulic fracturing as the initiation and propagation of tensile fractures and 2) hydraulic
155 shearing, i.e., the reactivation of existing discontinuities in shear with associated irreversible
156 dilation that is often referred to as the self-propping mechanism. Hydraulic shearing is of



157 particular relevance for EGS as it has been shown that slip along fractures can generate a
158 permeability increase by up to 2-3 orders of magnitude (Jupe et al., 1992, Evans et al., 2005a;
159 Häring et al., 2008). If the rock mass in the reservoir is stressed to a critical level (e.g.,
160 Byerlee 1978), then a relatively small reduction of effective normal stress would be sufficient
161 to cause shearing along pre-existing discontinuities that are optimally-oriented for failure
162 (Hubbert and Rubey, 1959; Rayleigh et al., 1976; Zoback and Harjes 1997; Evans et al.,
163 1999; Evans, 2005). Thus, shearing and the associated permeability enhancement can occur at
164 large distances from the injection point, even though the causal pressure increases may be low
165 (Evans et al., 1999; Saar and Manga, 2003; Husen et al., 2007). In contrast, hydraulic fracture
166 initiation and propagation (i.e., the original concept of EGS to connect two boreholes)
167 requires high pressures exceeding the minimum principal stress to propagate hydro-fractures
168 away from the wellbore. The high pressure in the fracture may interact with natural fractures
169 and stimulate them, leading to leak-off (i.e., the extent of hydro-fractures is influenced by
170 pressure losses and the existence of pre-existing fractures). Therefore, hydraulic fracturing is
171 often only considered relevant in the near-field of a wellbore, where it improves the linkage
172 between the borehole and the natural fracture system. Rutledge et al., (2004) showed that
173 shear activation of existing fractures and creation of new fractures can occur concomitantly,
174 dependent on the in-situ stress conditions, injection pressure, initial fracture transmissivity,
175 fracture network connectivity and fracture orientation (e.g., McClure and Horne, 2014).
176 Regardless of which process is dominant, the direction of reservoir growth, and therefore, the
177 geometry of the stimulated volume, depends to a considerable degree on the in-situ stress
178 gradient, stress orientation and the natural fracture network.

179 Pressurized fractures may open due to a reversible compliant response to pressure (Rutqvist
180 1995; Rutqvist and Stephansson 2003; Evans and Meier, 2003), or due to largely irreversible
181 shear dilation (Lee and Cho 2002; Rahman et al., 2002). As a consequence of the coupling
182 between pressure, fracture compliance and permanent fracture aperture changes, the pressure
183 field does not propagate through the reservoir as a linear diffusive field, but rather as a
184 pressure front (Murphy et al., 2004). The fracture normal and shear dilation that occurs in
185 response to elevated fluid pressure thus has a major influence on the magnitude and profile of
186 the propagating pressure perturbation in the rock mass during hydraulic stimulations (Evans
187 et al., 1999; Hummel and Müller, 2009). As a consequence, fracture compliance and
188 normal/shear dilation characteristics have an impact on the size and geometry of the reservoir
189 created during hydraulic stimulation.



190 Although the aforementioned processes are conceptually well understood, the quantification
191 and detailed understanding required for designing stimulations and truly engineering
192 geothermal reservoirs are insufficient. There remains considerable uncertainty as to how the
193 above processes interact, and what rock mass characteristics and injection metrics control the
194 dominant mechanisms (Evans et al, 2005a; Jung 2013). Thermo-hydro-mechanically coupled
195 numerical models have become widely used for analysing relevant aspects of reservoir
196 stimulation in retrospective (e.g., Baujard and Bruel, 2006; Rutqvist and Oldenburg 2008;
197 Baisch et al., 2010; Gischig and Wiemer, 2013) or as prospective tools for predicting
198 reservoir behaviour or alternative stimulation strategies (e.g., McClure and Horne 2011; Zang
199 et al., 2013; Gischig et al., 2014; McClure 2015; Yoon et al., 2015). The fact that such
200 numerical models must be parameterized from sparse quantitative field-scale data is a major
201 limitation of all those studies. In the following we present an overview of the experimental
202 observations of hydro-mechanical coupling that are relevant to the parameterization of
203 numerical models. These stem from reservoir-scale (i.e. hectometre) stimulation operations,
204 such as in EGS demonstration projects or oil and gas reservoirs, intermediate-scale (i.e.,
205 decametre) in-situ-experiments, and small-scale laboratory experiments.

206

207 2.1.1 Reservoir-scale experiments

208 The paucity of high-quality data on the stimulation process from reservoir-scale projects is
209 largely because they tend to be conducted at depths of several kilometres, which prohibits the
210 observation of hydro-mechanical processes from instrumentation installed within the
211 reservoir. In the geothermal domain, such projects constitute expensive experiments and thus
212 are relatively few in number, whereas, in the oil and gas domain, where hydrofracture
213 operations are frequent and routine, the data tend to be proprietary. Nevertheless, some
214 notable datasets have been acquired for deep brine injection projects (Ake et al., 2005; Block
215 et al., 2015), deep scientific drilling projects such as the German KTB project (Zoback and
216 Harjes 1997; Emmermann and Lauterjung 1997; Jost et al., 1998; Baisch and Harjes 2003),
217 hydraulic fracturing for oil & gas production enhancement (Warpinski 2009; Das and Zoback
218 2011; Dusseault et al., 2011; Pettitt et al., 2011; Vermeylen and Zoback 2011; Boroumand and
219 Eaton 2012; van der Baan et al., 2013; Bao and Eaton 2016;), and during the stimulation of
220 deep geothermal boreholes (Parker, 1989; Jupe et al., 1992; Cornet & Scotti, 1993; Tezuka &
221 Niitsuma, 2000; Asanuma et al., 2005; Evans et al., 2005a; Häring et al., 2008; Brown et al.,
222 2012; Baisch et al., 2015;). Well-documented hydraulic stimulation datasets generally



223 include microseismic observations as well as injection pressures and flow rates and
224 occasionally, tilt monitoring (Evans, 1983; Warpinski et al., 1997). Although much
225 information can be gained from these datasets, including imaging of microseismic structures
226 (Niitsuma et al. 1999; Maxwell, 2014), energy balance between injected fluids and seismic
227 energy release (Boroumand and Eaton 2012; Zoback et al., 2012; Warpinski et al., 2013), and
228 source mechanisms (Jupe et al., 1992; Deichmann and Ernst, 2009; Warpinski and Du 2010;
229 Horálek et al, 2010), the constraints placed on the processes are insufficient to resolve details
230 of the hydro-mechanical processes that underpin permeability enhancement, flow-path
231 linkage, channelling, or the interaction with natural fractures. Moreover, it is likely that a
232 significant part of the permeability creation processes take place in an aseismic manner
233 (Cornet et al., 1997; Evans et al., 1998; Guglielmi et al., 2015b; Zoback et al., 2012). In many
234 deep hydraulic stimulation projects the rock mass is only accessed by one or at most a few
235 boreholes, and the structural and geological models of the reservoir are not well defined. In
236 general, the displacements on fractures arising from the injection can only be directly
237 measured where they intersect the boreholes, and deformation occurring within the rock mass
238 is poorly resolved.

239 Despite limitations in reservoir characterization and monitoring, significant insights into the
240 stimulation process can be gleaned from the experience from the EGS projects that have been
241 conducted to date. Two examples are studies of stimulation-induced fault slip and changes of
242 flow conditions in the fracture network associated with the permeability creation processes at
243 the Soultz-sous-forêt (Cornet et al., 1997; Evans et al., 2005b) and the Basel EGS projects
244 (Häring et al., 2008). At both sites, it has been shown that permeability in the near-wellbore
245 region increased by 2-3 orders of magnitude. At Basel, a single initially-impermeable fracture
246 has been shown to take at least 41% of the flow during the 30 l/s injection stage (Evans and
247 Sikaneta, 2013), whereas at Soultz-sous-forêt, the stimulation of the 3.5 km reservoir served
248 to enhance the injectivity of a number of naturally-permeable fractures (Evans et al., 2005b).
249 These fractures tended to be optimally oriented for fault slip, as also found elsewhere by
250 Barton et al. (1995, 1998) and Hickman et al. (1998). At Soultz-sous-forêt, it was possible to
251 estimate stimulation-induced slip and normal opening of fractures that cut the borehole by
252 comparing pre- and post-stimulation acoustic televiewer logs (Cornet et al., 1997; Evans et
253 al., 2005). Shearing of fractures was also proposed as the predominant mechanism of
254 permeability enhancement at the Fjällbacka site in Sweden, by Jupe et al. (1992), based upon
255 focal mechanism analysis. The above observations provide evidence of a link between
256 shearing and permeability changes.



257 An additional, important lesson from deep stimulation projects is that the stress conditions in
258 reservoirs may be strongly heterogeneous, and that this influences the flow field (e.g.
259 Hickman et al, 2000). For instance, profiles of horizontal stress orientation defined by
260 wellbore failure observations commonly show significant fluctuations whose amplitude varies
261 systematically with scale (Shamir and Zoback, 1992; Valley and Evans 2009; Blake and
262 Davatzes, 2011), even though that may have an average trend consistent with the tectonic
263 stress field. Strong deviations may occur in the vicinity of faults, indicating past fault slip and
264 complex fault zone architecture (Valley and Evans, 2010; Hickman et al., 2000). Similarly,
265 the hydro-mechanical properties of faults depend on the fault architecture, which itself
266 depends on lithology and the damage history accumulated over geological time (Caine et al.,
267 2006, Faulkner and Rutter 2008; Guglielmi et al., 2008, Faulkner et al., 2010, Jeanne et al.,
268 2012). Within a fault zone, permeability and compliance contrasts can vary by several orders
269 of magnitude (Guglielmi et al., 2008), thus complicating the predictability of hydro-
270 mechanical responses to stimulations. In some EGS projects, it was observed that the
271 hydraulic communication between injection and production boreholes may be unsatisfactory
272 for efficient exchange of heat, either because of high flow impedance, such as at Ogachi,
273 Japan, (Kaieda et al., 2005), or because of flow channelling, as inferred from early thermal
274 drawdown at Rosemanowes, UK (Nicol and Robinson, 1990), and Hijiori, Japan (Tenma et
275 al., 2008).

276

277 2.1.2 Laboratory-scale experiments

278 On the laboratory-scale, considerable effort has been devoted to experiments that address the
279 role of effective stress changes on normal fracture opening and closure, shear dilatancy and
280 related permeability changes (Goodman 1974; Bandis et al., 1983; Yeo et al., 1998; Esaki et
281 al., 1999; Gentier et al., 2000; Olson and Barton, 2001). These experiments have
282 demonstrated that the relationships between fluid pressure change, fracture opening and flow
283 within rough natural fractures are strongly non-linear. Even though significant progress has
284 been made on defining permeability changes during normal opening and shear slip on the
285 laboratory scale, the non-linear relationships between fracture opening, changes in effective
286 normal stress, shearing, and the resulting permeability are yet not well constrained (Esaki et
287 al., 1991; Olsson et al., 2001, Vogler et al., 2015). One common approach is to represent the
288 fracture as two parallel plates whose separation, the hydraulic aperture, gives the same flow
289 rate per unit pressure gradient as would apply for the natural fracture. For parallel plates and



290 laminar flow, the flow rate per unit pressure gradient is proportional to the cube of hydraulic
291 aperture. However, for rough-walled fractures, the hydraulic aperture, a_h , is generally only a
292 fraction of the mean mechanical aperture, a_m (i.e. the mean separation of two surfaces), the
293 fraction tending to decrease with smaller apertures, although the precise relationship is
294 difficult to derive from fracture geometry alone (Esaki et al., 1999; Olsson and Barton 2001;
295 Vogler et al., 2015). At larger mechanical apertures, limited evidence suggests that an
296 incremental form of the cubic law might hold such that changes in mechanical aperture give
297 rise to equal changes in hydraulic aperture, at least for normal loading (e.g., Schrauf and
298 Evans, 1986; Evans et al. 1992; Chen et al., 2000). For shear-induced dilation, an additional
299 complication arises from channel clogging due to gouge production (e.g. Lee et al., 2002).
300 Deviations from the cubic law also occur when flow becomes non-laminar, which tends to
301 occur at high flow velocities (Kohl et al., 1997), or at feed points in boreholes (e.g. Hogarth et
302 al., 2013; Houben, 2015).

303 Dilatancy associated with shearing is often expressed in terms of a dilation angle, which is a
304 property describing the relationship between mean mechanical aperture and slip. Dilation
305 angle depends on the fracture surface characteristics, the effective normal stress and the
306 amount of slip. Particularly important within the stimulation context is the dependence of
307 dilation on effective normal stress, the dilation angle tending to decrease at higher effective
308 normal stress, in large part because shorter wavelength asperities are sheared off (Evans et al.,
309 1999). Thus, shearing-induced dilation is likely to be more effective at low effective normal
310 stress, such as in the near field of the injection where fluid pressures are relatively high.
311 Clearly, insights from laboratory experiments into the relationships describing fracture
312 dilation and permeability changes are important for understanding field observations in EGS
313 reservoirs (e.g., Robinson and Brown; 1990), and also for parametrizing numerical models.

314

315 2.1.3 Intermediate-scale experiments

316 In-situ experiments at the intermediate-scale (i.e., decameter-scale) serve as a vital bridge
317 between laboratory and reservoir scales. As such, they can contribute to an improved
318 understanding of reservoir behaviour during stimulation, and to enable up-scaling of hydro-
319 mechanical information obtained from laboratory experiments (Jung, 1989; Martin et al.,
320 1990; Rudquist, 1995; Schweisinger et al., 1997; Cornet et al., 2003; Murdoch et al., 2004,
321 Cappa et al., 2006; Derode et al., 2013; Guglielmi et al., 2014; 2015). Much experience has
322 been gained from stress testing using the hydraulic methods of hydro-fracturing (HF),



323 hydraulic testing of pre-existing fractures (HTPF) (Haimson and Cornet, 2003), and hydro-
324 jacking (Evans and Meier, 1995; Rutqvist and Stephansson, 1996). Hydraulic tests have been
325 commonly used to quantify pressure-sensitive permeability changes (Louis et al., 1977), and
326 normal stiffness in natural fractures or faults (Rutqvist et al., 1998). Evans and Wyatt (1984)
327 estimated the closure of a fracture zone from observed surface deformations induced by
328 drilling-related drainage of fluid pressure within the structure. Similarly, Gale (1975), Jung
329 (1989), Martin et al. (1990), Guglielmi et al. (2006), and Schweisinger et al. (2009) used
330 borehole caliper sondes to monitor changes in fracture aperture and pressure during hydraulic
331 jacking tests. The resulting displacements and the flow and pressure responses allowed
332 relationships between mechanical and hydraulic aperture changes to be established and helped
333 to constrain the fracture/fault normal compliance at larger scales.

334 Irreversible permeability increases arising from slip-induced dilation of natural fractures are
335 particularly relevant for stimulation of EGS and hydrocarbon reservoirs. To study the
336 phenomenon in-situ, Guglielmi et al. (2014) developed a novel double packer system
337 (SIMFIP) that allows the simultaneous measurement of pressure, flow rates and 3-
338 dimensional relative displacements occurring across a fracture isolated within the interval in
339 response to injection. The device was successful in reactivating a fault zone in a limestone
340 formation in Southeast France (Derode et al., 2013; Guglielmi, et al., 2015). Pressure,
341 injection rate and 3D displacements in the SIMFIP interval were measured, together with
342 microseismic activity, tilt and fluid pressure in the vicinity of the injection borehole. The
343 dataset is unique, and provided quantitative insights into the relationships between (i) fault
344 dislocation including shear and permeability changes, (ii) fault normal compliance and static
345 friction, and (iii) slip velocities and magnitudes and their relation to aseismic and seismic slip.
346 Recently, a similar experiment was conducted in a series of interacting complex fault zones in
347 shale (Guglielmi et al., 2015). Distributed pore pressure and strain sensors across the faults
348 allowed the evolution of the pressurized and slipped areas to be constrained, which was not
349 previously possible. Such experiments provide a useful methodology for advancing our
350 understanding of the hydro-mechanical coupled processes in complex faults.

351

352 2.2 Hydraulic fracturing experiments

353 Experience gained from large scale stimulation of EGS reservoirs in crystalline rock suggests
354 that hydraulic shearing is the dominant mechanism for permeability creation, at least remote
355 from the injection point. However, the initiation and propagation of hydraulic fractures may



356 be an important mechanism in the near field of the wellbore to connect the wellbore to the
357 pre-existing fracture network in the reservoir (Cornet and Jones, 1994). Considerable effort
358 has been devoted to understand the initiation and propagation of hydraulic fractures on both
359 the laboratory and intermediate field scale.

360

361 2.2.1 Laboratory scale hydraulic fracturing experiments

362 Many well-controlled, small-scale laboratory experiments on hydrofracture are documented in
363 the literature (Jaeger 1963; Zoback et al., 1977; Warpinski et al., 1982; Bruno and Nakagawa
364 1991; Johnson and Cleary 1991; Song et al., 2001; Jeffrey and Bunger 2007; Bunger et al.,
365 2011). For such experiments, samples of various shapes (e.g., hollow cylinders and perforated
366 prisms) are loaded along their boundaries and the internal fluid pressure is increased until a
367 hydraulic fracture initiates and propagates. For some tests, transparent material like
368 polymethylmethacrylate (PMMA) were used to image fracture growth. Some experimental
369 setups include multi-material "sandwiches" to study the effect of stress contrast on hydraulic
370 fracture containment (Jeffrey and Bunger 2007; Warpinski et al., 1982). Others study the
371 interaction of propagating hydrofractures with pre-existing fractures (Zoback et al., 1977;
372 Meng, 2011; Hampton et al, 2015) or rock textures (Ishida 2001; Chitrala et al., 2010), the
373 impact of injection fluids with different viscosities (Bennour et al., 2015) or the role of stress
374 anisotropy (Doe and Boyce, 1989) on the geometry and orientation of generated fractures, or
375 the interaction between multiple fractures (Bunger et al., 2011). These laboratory studies
376 provide important results relevant for EGS. For instance, in the common situation where a
377 family of natural fractures is not normal to the minimum principal stress, injections with high
378 viscosity fluids (viscosity dominated regime) may help maintain tensile fracture propagation
379 normal to the minimum principal stress despite the presence of cross-cutting fractures
380 (Zoback et al., 1977), whereas low viscosity fluids (toughness dominated regime) such as
381 water will promote leak-off into the cross-cutting natural fractures, whose permeability may
382 be increased by shear (Rutledge et al, 2003). This leak-off will tend to limit hydrofracture
383 propagation. Laboratory studies also give insights into the influence of shear stress shadow
384 and transfer on hydraulic fracture growth (Bunger et al., 2011). Laboratory tests have also
385 been essential for providing well-controlled fracture initiation and propagation datasets to
386 benchmark hydraulic fracture simulation codes (Bunger et al., 2007).

387



388 2.2.2 Intermediate scale hydraulic fracturing experiments

389 Intermediate scale experiments have been performed to study initiation and propagation of
390 hydraulic fractures. Typically, they are conducted from boreholes drilled from excavations to
391 facilitate dense near-field instrumentation and secure good experimental control. An early
392 example is the series of experiments that took place at the Nevada Test Site in soft, bedded
393 volcanic tuff with high porosity and high permeability (Warpinski, 1985; Warren and Smith,
394 1985). The pressure, flow and fracture aperture were monitored during the experiments, and
395 the fractures were mined back at the end of the experiments. The mine back revealed that
396 stress contrasts were the predominant influence on hydraulic fracture containment, and that
397 the fractures consisted of multiple fracture strands and thus differed significantly from simple
398 shapes assumed in theoretical studies. This complexity of the fracture shape impacts the flow
399 and pressure distribution within the propagating hydraulic fractures. Another notable series of
400 in-situ tests on hydraulic fracture propagation within the context of coal-seam mining and
401 block cave mine preconditioning have been performed by the hydraulic fracture group of
402 CSIRO (Chacón et al., 2004; Jeffrey et al., 1993; 1992, 2009; Jeffrey and Settari 1995; van As
403 et al., 2004; van As and Jeffrey 2002, 2000). The block cave mining experiments were
404 performed in hard rock media and thus are the more relevant to EGS. Those conducted in the
405 quartz monzonite porphyries at the Northparkes mine in Australia are probably the most
406 detailed and densely instrumented tests executed to date, and included tiltmeter monitoring, a
407 micro-seismic network, and pore pressure sensors as well as detailed rock mass and stress
408 characterization. Hydrofractures were formed with water and cross-linked gels, with coloured
409 plastic proppants added in order to facilitate their identification once the test volume was
410 mined back. The mapped trajectories of the hydraulic fractures exhibited complex geometries,
411 sometimes with multiple branching and crossing of joints, veins and shear zones, with and
412 without offset. Sub-parallel propped sections accounted for 10 to 15% of the total fracture
413 extent, which microseismic activity indicated was more than 40 m from the injection point.
414 The results demonstrate that the geometry of the fractures is much more complex than
415 typically obtained in small scale laboratory experiments in a homogeneous material and
416 uniform stress field. The complexity close to the injection point is controlled by the near-well
417 stress perturbation and the interaction with natural fractures and rock mass fabric.

418 Natural fractures have also a strong influence on the propagation of hydraulic fractures. The
419 propagation regime (i.e. viscosity-dominated or toughness-dominated (Detournay, 2016)) can
420 be controlled by the injection rate and injected fluid rheology and will have likely a strong
421 influence on the interaction with natural fractures and the final complexity of the hydraulic



422 fractures, although this has not been validated by in-situ experiment. Another relevant aspect
423 that has not been investigated with in-situ tests is the problem of proppant transport and
424 distribution within the created fractures. Indeed, in the case of hydraulic fractures, the self-
425 propping mechanism, which results in a permanent aperture increase, is unlikely to be
426 effective, and so proppant placement is necessary for insuring permanent permeability
427 enhancement. Finally, the nature of the microseismicity generated by hydraulic fracturing is
428 not adequately understood. Moment tensor analyses can offer insight into the nature of the
429 failure in a microseismic event (Warpinski and Du, 2010; Eyre and van der Baan, 2015). For
430 example, they can help resolve whether the seismic radiation is primarily generated by shear
431 on pre-existing fractures that are intersected by the propagating fracture, with relatively little
432 energy generated by the advancing mode I tip of the hydraulic fracture (Sileny et al, 2009;
433 Horálek et al, 2010; Rutledge et al., 2004).

434

435 2.3 Rock mass deformation and stress interaction

436 Injection of fluid into a rock mass invariably leads to deformation of the surrounding rock
437 mass due to poroelasticity (Biot 1941) or slip-related stress changes (McClure and Horne
438 2014). Numerical studies have suggested that stress interaction between adjacent fractures can
439 have a significant impact on the stimulation results (e.g., Preisig et al., 2015; Gischig and
440 Preisig 2015). In most reservoir stimulations, the microseismic clouds exhibit an oblate shape,
441 due primarily to the interaction between the strongly anisotropic stress field with the natural
442 fracture population. This tendency to form an oblate ellipsoidal shape instead of a sphere may
443 also be promoted by stress transfer from slipped fractures which tends to inhibit slip on
444 neighbouring fractures (Gischig and Preisig 2015). Schoenball et al. (2012) and Catalli et al.
445 (2013) have demonstrated that induced earthquakes preferably occur where stress changes
446 generated by preceding nearby earthquakes render the local stress field to be more favourable
447 for slip. Similar effects have been observed for natural earthquakes (Stein 1999). The effect
448 becomes more important during stimulation as time goes on, especially at the margin of the
449 seismicity cloud. Direct observation of deformation associated with fluid injection has been
450 observed in several intermediate-scale in-situ experiments. Evans and Holzhausen (1983)
451 report several case histories of using tiltmeter arrays to observe ground deformation above
452 high pressure hydraulic fracturing treatments. The results show clear evidence of self-
453 propping of the induced fractures. van As et al. (2004). Jeffrey et al (2009) used a tiltmeter
454 array to monitor a hydrofracturing treatment at the Northparkes mine in Australia. The pattern



455 of tilting indicated the induced fracture was sub-horizontal, which was confirmed by
456 excavating the fracture traces. Evans and Wyatt (1984) modelled strains and tilts occurring
457 around a well during air drilling and found the deformation was due to opening of a pre-
458 existing fracture zone in response to fluid pressure changes. Derode et al. (2013) observed
459 tilts of 10^{-7} - 10^{-6} radians some meters away from small volume injections into a fault in
460 limestone. In contrast, Cornet and Deroches (1990) monitored surface tilts with a 6 instrument
461 array during injections of up to 400 m³ of slurries into granite at 750 m depth at the Le Mayet
462 test site in France and report no resolved signal associated with the injections.

463 Rock mass deformation during stimulation injections necessarily leads to stress changes in the
464 rock mass. Small but non-zero residual stress changes induced by hydraulic fracturing were
465 measured using a stress cell by van Ass et al. (2004). Stress changes during injections are
466 recognized as playing a potentially important role in determining the pattern of fracture and
467 slip that develops during the injection (e.g. Preisig et al., 2015; Catalli et al, 2013).

468

469 2.4 Seismic and aseismic slip

470 A significant fraction of the slip that occurs on fractures within a reservoir undergoing
471 stimulation may be aseismic, depending upon in-situ stress and geological conditions. That
472 aseismic slip has occurred is often inferred indirectly from changes in the hydraulic
473 characteristics of a reservoir without attendant micro-seismicity (Scotti and Cornet 1994;
474 Evans, 1998). Direct detection of aseismic slip is difficult as it requires relative displacements
475 across fractures to be resolved from borehole or near-field deformation measurements (e.g.,
476 Maury 1994; Cornet et al., 1997, Evans et al., 2005b). For example, Cornet et al. (1997)
477 compared borehole geometry from acoustic televiewer logs run before and after the 1993
478 stimulation at the Soultz-sous-forêt site and found that 2 cm of slip had apparently occurred
479 across a fracture. The cumulative seismic moment of events in the neighbourhood of the
480 fracture was insufficient to explain the observed slip magnitude, thereby suggesting a large
481 portion of the slip had occurred aseismically. Indeed, almost all fracture zones that were
482 hydraulically active during the stimulation showed evidence of shear and opening-mode
483 dislocations of millimetres to centimetres (Evans et al. (2005b).

484 The transition from aseismic to seismic slip was directly observed by Guglielmi et al. (2015)
485 during fluid injection into a well-instrumented fault in limestone in a rock laboratory at 280 m
486 depth. Some 70% of a 20-fold permeability increase occurred during the initial aseismic slip
487 period. The transition to seismic slip coincided with reduced dilation, and the inference that



488 slip zone area exceeded the pressurized area, suggesting the events themselves lay outside the
489 pressurized zone. Modelling the observed slip as occurring on a circular fracture with total
490 stress drop gave a radius of 37 m and a moment release of $65e9$ Nm, far larger than the
491 estimated seismic moment release of the order of $1e6$ Nm, again indicating most slip was
492 aseismic. Guglielmi et al. (2015) concluded that the aseismic behaviour is due to an overall
493 rate-strengthening behaviour of the gauge filled fault and seismicity occurs due to local
494 frictional heterogeneity and rate-softening behaviour. These results are consistent with
495 laboratory experiments performed by Marone and Scholz (1988) on fault gauge which suggest
496 that slip at low effective normal stresses (as anticipated in the near field of a high-pressure
497 injection) and within thick gouge layers tends to be stable (aseismic).

498 Apart from these observations, aseismic slip has been mostly discussed from the perspectives
499 of semi-analytical or numerical models. Garagash and Germanovic (2012) used a slip-
500 weakening model to show that aseismic slip depends on the stress conditions and injection
501 pressure. Zoback et al. (2012) used McClure's (2012) rate-and-state friction model to show
502 that aseismic slip becomes more prominent for stress states farther from the failure limit.
503 Using the same model, Gischig (2015) demonstrated that slip velocity depends on fault
504 orientation in a given stress field. For non-optimally oriented faults, aseismic slip becomes
505 more prominent and the seismicity is less pronounced for lower slip velocities and shorter
506 rupture propagation distances. These model results suggest that aseismic slip and low slip
507 velocities may be promoted by avoiding the stimulation of optimally oriented critically-
508 stressed faults. Clearly, a more detailed understanding of the conditions that result in aseismic
509 slip may be a basis for less hazardous stimulations.

510

511 2.5 Induced seismicity

512 Keeping induced seismicity at levels that are not damaging or disturbing to the population
513 continues to be a major objective for EGS (Giardini, 2009; Bachmann et al., 2011; Majer et
514 al., 2012; Evans et al., 2012) and other underground engineering projects (oil and gas
515 extraction, liquid waste disposal, gas and CO₂ storage). Man-made earthquakes are not a new
516 phenomenon (Healy et al. (1968), McGarr, 1976; Pine et al., 1987; Nicholson and Wesson,
517 1990, Gupta, 2003). However, the occurrence of several well-reported felt events near major
518 population centres has served to focus attention on the problem (Giardini, 2009; Ellsworth
519 2013; Davies et al., 2013; Huw et al., 2014; Bao and Eaton, 2016). Some even led to
520 infrastructure damage, such as followed the Mw5.7 event in Oklahoma, USA (Keranen et al.,



521 2013), or the suspension of the projects (e.g., the geothermal projects at Basel (Häring et al.,
522 2008) and St. Gallen (Edwards et al., 2014) in Switzerland. As a consequence, a substantial
523 research effort has been initiated to understand the processes that underlie induced seismicity.
524 Examples are the numerous studies that have been performed using the high-quality seismic
525 dataset collected during the Basel EGS experiment. Dyer et al. (2010), Kraft and Deichmann
526 (2014) and Deichmann et al. (2014) analysed waveforms of the seismicity to determine
527 reliable source locations. Terekawa et al. (2013) used an extended catalogue of the focal
528 mechanism solutions of Deichmann and Ernst (2009) to estimate the stress field at Basel and
529 to infer the pore pressure increase required to trigger the events. Goertz-Allmann et al. (2011)
530 determined stress drop for the Basel seismicity and found higher stress drops at the margin of
531 the seismic cloud than close to the injection borehole. A similar dependency for Gutenberg-
532 Richter b-values was found by Bachmann et al. (2012) – lower b-values tended to occur at the
533 margin of the seismicity cloud and at later injection times.

534 There are numerous analyses of induced seismicity at other EGS sites. Pearson (1981) and
535 Phillips et al (1997) analysed microseismicity generated during the stimulation of the 2930 m
536 deep ‘large Phase 1’ and the 3460 m deep Phase 2 reservoirs respectively at the Fenton Hill
537 EGS site, New Mexico. Bachelor et al. (1983) and Baria and Green (1986) summarize
538 microseismicity observed during the stimulation injections into the Phase 2a and 2b reservoirs
539 at Rosemanowes in Cornwall, UK. Tezuka and Niitsuma (2000) examined clusters of
540 microseismic events generated during the stimulation of the 2200 m deep reservoir at the
541 Hijiori EGS site in Japan. Baisch et al. (2006, 2009, 2015) analysed data from different stages
542 of the stimulation of the Habanero EGS reservoir in the Cooper Basin, Australia. Calò et al.
543 (2011) used microseismicity generated during the stimulation of the 5 km deep EGS reservoir
544 at Soultz-sous-forêt to perform time-lapse P-wave tomography to infer pore pressure
545 migration during injection.

546 Another major focus of induced seismicity research has been the development of hazard
547 assessment tools for injection related seismicity. The primary goal of these efforts is to
548 develop a dynamic, probabilistic and data-driven traffic light system that can provide real-
549 time hazard estimates during injections (Karvounis et al., 2014; Kiraly et al, 2016), as
550 opposed to the traditional, static traffic light system (Bommer et al., 2006). Bachmann et al.
551 (2011) and Mena et al. (2013) developed several statistical models and tested them in pseudo-
552 prospective manner using the Basel seismicity dataset. More complex models including
553 physical considerations and stochastic processes (so-called hybrid-models) were developed to
554 include information on the reservoir behaviour and from the spatio-temporal evolution of



555 seismicity (Goertz-Allmann and Wiemer, 2013; Gischig and Wiemer, 2013; Kiràly et al.,
556 2016). Mignan et al. (2015) evaluated reported insurance claims arising from the Basel
557 induced seismicity in order to infer procedures for evaluating risk based on induced seismic
558 hazard estimates.

559 The Gutenberg-Richter b-value, which describes the reduction in the frequency of occurrence
560 of events with increasing earthquake magnitude, plays a key role in induced seismic hazard
561 analysis. Schorlemmer et al. (2005) examined the b-values of earthquakes in different stress
562 regimes and found lower values correlated with areas of higher differential stress. Similar
563 trends have been reported for induced seismicity (Bachmann et al., 2012), but also in tectonic
564 earthquakes (Tormann et al., 2014; Torman et al., 2015; Spada et al., 2013) and laboratory
565 experiments (Amitrano 2003; Goebel et al., 2012). Thus, it was hypothesized that b-values are
566 related to local stress conditions (Scholz, 2015), or - in the context of induced earthquakes –
567 to a combination of pressure and stress conditions. Considering standard scaling laws between
568 magnitudes and earthquake source dimensions (i.e., slip and slipped area), it has to be
569 expected that seismicity with high b-values may have an indirect but strong impact on
570 permeability enhancement (Gischig et al., 2014). However, these observations have so far
571 only been qualitatively established, as the absolute stress state within the rock volume that
572 hosts the seismicity whose b-value is estimated has not been quantitatively determined.

573 Whilst the hazard associated with induced seismicity is clearly an important factor for
574 reservoir engineering, it should not be forgotten that the shearing of fractures and fracture
575 zones, which is the source of the seismicity, is a key process in the irreversible permeability
576 enhancement that is the objective of the stimulation injections. Furthermore, precise mapping
577 of the 3-D distribution of events provides an indication of the direction of fluid pressure
578 propagation and hence the geometry (i.e. size, shape, degree of anisotropy) of the distribution
579 of permeability enhancement – information that is vital for drilling subsequent well (Niitsuma
580 et al., 1999). Managing induced seismic hazard also requires considering the design of
581 reservoir attributes such as size, system impedance, and heat exchanger properties that control
582 system longevity (e.g., Gischig et al., 2014). Currently, few case studies consider both
583 seismicity and the related changes that occurred in the reservoir (e.g., Evans et al., 2005a),
584 and relatively few studies even report both permeability changes or well injectivity (e.g.,
585 Häring et al., 2008; Evans 2005b; Kaieda et al., 2005; Petty et al., 2013). More work is
586 needed to quantitatively link the spatial, temporal or magnitude distribution of seismicity with
587 the thermo-hydraulic-mechanical properties of the rock mass under stimulation conditions.



588 We believe controlled experiments on the intermediate (in-situ test site) scale supported by
589 laboratory-scale experiments could be key in making progress towards this end.

590

591 2.6 Open research question in hydraulic stimulation research

592 Research on reservoir stimulation for deep geothermal energy exploitation has been largely
593 performed through laboratory observations, large-scale projects, and numerical models.
594 Observations of full-scale reservoir stimulations have yielded important observations.
595 However, the difficulty in observing the processes occurring within the reservoir under
596 stimulation conditions severely limits the understanding of the permeability creation
597 processes in a way that aids future stimulation design.

598 Laboratory experiments are attractive because they are controllable and readily repeatable, but
599 they suffer from two main limitations: 1) Upscaling results to the field-scale is affected by
600 large uncertainties (Gale 1993). Although there is evidence that the roughness of fresh
601 fracture surfaces obeys well-defined scaling over many orders of magnitude (Power and
602 Tullis, 1991; Schmittbuhl et al., 1995), complications arise in upscaling the aperture
603 distribution and hence permeability of two semi-mated rough surfaces due to the effects of
604 damage and wear of the asperities during shearing and gouge formation (Amitrano and
605 Schmittbuhl, 2002; Vogler et al, 2016). 2) Laboratory tests are typically performed on single
606 fractures in relatively homogeneous materials and uniform stress conditions, which makes
607 upscaling to structures with multiple fractures such as fracture zones challenging. Similarly,
608 hydraulic fracture propagation behaviour is usually studied with homogenous rock samples
609 under uniform stress, and this can lead to an over-simplistic fracture flow and/or hydraulic
610 fracture propagation behaviour. In an EGS reservoir, for example, the stress may be
611 heterogeneous on the meter to decametre-scale (Evans et al., 1999; Valley and Evans 2009;
612 Blake and Davatzes, 2011), and the rock mass may contain various heterogeneities such as
613 stiffness contrasts, fractures or faults (Ziegler et al., 2015).

614 Because of the large uncertainties in upscaling, many numerical studies make direct (i.e. not
615 upscaled) use of laboratory results to parameterize HM-coupled models for EGS, because so
616 few field-scale relationships are available (e.g., Rutqvist, 2011; McClure, 2012; Gischig et al.,
617 2014). This impacts the reliability of the numerical simulation studies, because the
618 descriptions of the processes and the input parameter values may be inappropriate for the
619 scale of the simulation.



620 Clearly there is a need for field-scale hydraulic stimulation experiments that bridge the
621 various scales, and are performed with the target rock mass equipped with a comprehensive
622 monitoring system to capture details of the processes. Recently several intermediate-scale
623 hydro-shearing and hydrofracturing experiments have been performed in a densely
624 instrumented rock mass (i.e., Guglielmi et al., 2008, 2014 and 2015; Jeffrey et al., 2009). The
625 hydro-shearing experiments by Guglielmi et al. (2008) have all been in sedimentary rock
626 types at shallow depth. No such densely-instrumented experiments have been performed in
627 fractured and faulted crystalline basement rocks faults, the target rocks for most EGS, where a
628 variety of complex fault architectures and stress-fracture system configurations need to be
629 investigated. The on-going In-situ Stimulation and Circulation (ISC) experiment tries to
630 contribute to the filling of this research gap. In particular, the experiment addresses the
631 following research questions:

- 632 [1] What is the relationship between pressure, effective stress, fracture aperture, slip,
633 permeability and storativity?
- 634 [2] How does the transient pressure field propagate in the reservoir during stimulation?
- 635 [3] How does the rock mass deform as a result of rock mass pressurization, fracture
636 opening and/or slip?
- 637 [4] How does stress transfer inhibit or promote permeability enhancement and seismicity
638 along neighbouring fractures?
- 639 [5] Can we quantify the transition between aseismic and seismic slip and the friction
640 models (such as rate-and-state friction) describing slip evolution and induced
641 seismicity?
- 642 [6] How do hydraulic fractures interact with pre-existing fractures and faults and how can
643 the interaction be controlled?
- 644 [7] How does seismicity evolve along faults and fractures of different orientation?
- 645 [8] How does induced seismicity along stimulated faults compare to induced seismicity
646 along newly created hydraulic fractures?
- 647 [9] Can we quantify the link between spatial, temporal and magnitude distribution and
648 HM coupled properties of fractures and faults?

649

650 3 The ISC experiment

651 The objective of the ISC experiment is to contribute in finding answers to the above
652 mentioned research questions by 1) stimulating a naturally fractured crystalline rock volume



653 at the decameter scale that is exceptionally well characterized in terms of its structural,
654 geomechanical, and hydraulic conditions and 2) providing a dense network of sensors within
655 the test volume so as to establish a 3D data set at high spatial resolution that will yield
656 detailed insight into geomechanical processes associated with induced micro-earthquakes,
657 fracture shearing, permeability creation and fluid circulation.

658

659 3.1 The in-situ rock laboratory

660 The ISC experiment is being performed at the Grimsel Test Site (GTS), near the Grimsel Pass
661 in the Swiss Alps (Figure 1a). The GTS is owned by the National Cooperative for the
662 Disposal of Radioactive Waste (NAGRA), and was developed as a facility to host in-situ
663 experiments relevant to nuclear waste repository research. The facility consists of a complex
664 of tunnels at a mean depth of 480 m that penetrate crystalline rock with well-documented
665 structures. The rock type is considered representative for the Alpine crystalline basement that
666 is a main target for EGS. The test site for the ISC experiment is located in the southern part of
667 the GTS (marked in blue in Figure 1b) between a Tunnel that is called AU Tunnel in the west
668 and the VE Tunnel in the east.

669 The rock at the GTS consists of Grimsel granodiorite and Central Aar granite. Both show an
670 alpine foliation that strikes NE and dips steeply at $\sim 77^\circ$ towards SE. The moderately fractured
671 rock mass is intersected by ductile and brittle shear zones, as well as brittle fractures and
672 metabasic dykes. Within the ductile shear zones, numerous fractures that are commonly
673 partially filled with gouge are present. Three shear zone orientations can be distinguished at
674 the GTS (Keusen 1989). The S1 shear zones are parallel to the alpine foliation with an
675 orientation of 142/77 (i.e. dip-direction/dip). The S2 shear zones are slightly younger than S1
676 and oriented with 157/75 (Keusen et al., 1989a). Shearing of the S2 structures has led to
677 minor folding of the S1 structures (Wehrens, 2015). The youngest shear zone direction (so-
678 called S3), have E-W strikes and southward dips (183/65), and often show evidence of dextral
679 strike-slip movement. The target volume for the injections contains an S3 shear zone that is a
680 fracture zone bound by two metabasic dikes on either side, and that is intersected by three
681 ductile S1 shear zones.

682



683 3.2 Experimental Phases

684 The ISC experiment is divided into three phases (Figure 2). To answer all aforementioned
685 research questions a profound understanding of the local geology, hydrogeology, stress state
686 and rock mass properties is essential. Thus, the *first phase* is a pre-stimulation phase that aims
687 to characterize the rock volume in terms of geological / structural / stress conditions,
688 hydraulic and thermal properties, and fracture connectivity. In addition, during the pre-
689 stimulation phase, a monitoring system is established that allows capturing the seismo-hydro-
690 mechanical response at high spatial and temporal resolution that is necessary to address the
691 outlined research questions. The *second phase* - the main hydroshearing and hydrofracturing
692 experiment - is concerned with enhancing the permeability of the rock mass with high
693 pressure fluid injections. A *third and final phase*, the post-stimulation phase, is dedicated to
694 characterize the rock mass in great detail after stimulation to quantify changes in
695 permeability, fracture connectivity and heat exchanger properties.

696

697 3.2.1 Pre-Stimulation Phase – Rock mass characterization and Instrumentation

698 3.2.1.1 Boreholes, rock mass characterization and geological model

699 The governing aspects for designing the instrumentation of the decameter-scale ISC
700 experiment are 1) a detailed understanding of the geological settings in 3-dimensions (e.g.
701 fracture and fault orientation and intersections, fracture density, etc.) 2) the in-situ state of
702 stress, 3) the pre-stimulation hydraulic conditions, including the flow field, preferential fluid
703 flow path ways and transmissivities, 4) the borehole sections used for stimulation, 5) the type
704 of hydraulic injection (i.e. hydraulic shearing or hydraulic fracturing) and 4) anticipated
705 quantities and spatial distributions of strain, tilt and pressure within the rock volume during
706 stimulation.

707 During the pre-stimulation phase a series of 15 cored boreholes with a length between 18 and
708 50 m and diameters between 86 and 146 mm are drilled within or about the experimental
709 volume (Figure 3). Three boreholes are dedicated to stress measurements (SBH), two for the
710 stimulation injections (INJ), four for geophysical characterization and monitoring (GEO),
711 three for strain and temperature measurements (FBS) and another three for pore pressure,
712 strain and temperature measurements (PRP). The boreholes are characterized in terms of
713 geologic structures ,hydraulic properties and inter-borehole connectivity using various
714 geological (i.e. core logging), geophysical (i.e. optical televiewer logs, resistivity logs using a



715 guard resistivity sonde, full-wave sonic logs, ground penetrating radar (GPR) surveys with
716 unshielded antennas and active seismic measurements between the injection boreholes) and
717 single-hole and cross-hole hydraulic methods (i.e. packer tests such as pressure-pulse,
718 constant-rate and constant head injection tests, oscillating pumping tests, and tracer tests
719 using various solutes, DNA-encoded nanoparticles, and heat). In addition to borehole-based
720 characterization methods, the experimental rock volume was characterized using detailed
721 tunnel maps, reflection GPR from the tunnel walls and active seismic data acquisition
722 between the AU and VE tunnels (Figure 1b). The trajectories of the subsequent boreholes
723 were chosen on the basis of these preliminary geological and hydraulic data and simplified
724 numerical HM-coupled models (i.e. using 3DEC, Itasca 2014) for stimulation scenarios that
725 provide an estimate of the deformation field and pore pressure propagation along geological
726 structures.

727 The joint interpretation of the above geophysical borehole logging and imaging data, tunnel
728 mapping, core logging and hydraulic test data were used to constrain a 3D structural model of
729 the experimental volume (Krietsch et al., 2017). The 3D model illustrates the intersection of
730 the shear zones within the experimental volume (Figure 4). S1 shear zones (numbered from
731 north to south: S1.1 to S1.3) within the ISC test volume have similar orientations as the
732 overall foliation in the rock mass. These shear zones are characterized by an increase in
733 foliation intensity, and a few fractures with random distribution. The highest strains were
734 localized in mm-thick mylonitic bands. Due to similar appearance and orientation, no
735 distinction between S1 and S2 shear zones are made in the ISC volume. The experimental
736 volume is crosscut in east-west direction by two major (up to 1 m thick) meta-basic dykes that
737 are separated by 2 m. Within the ISC volume the S3 shear zones have the same orientation as
738 the meta-basic dykes. Thus, each of the two shear zones (here referred to as S3.1 and S3.2) is
739 localized along the major meta-basic dykes. Shearing of the meta-basic dykes appears to have
740 been localized in fine ductile shear bands resulting in biotite-rich mylonitic shear bands (i.e.
741 1-2 cm thick). The dextral shearing of S3 led to a deformation of S1 faults around the meta-
742 basic dykes (Figure 4). Multiple persistent, partly open fractures are located between and
743 within the meta-basic dykes and within the host rock close to the fault. The volume between
744 the two sheared dykes is characterized by a high brittle fracture density (i.e. more than 20
745 fractures per m) compared to the rest of the rock mass (0-3 fractures per meter; Krietsch et al.,
746 2017). The orientations of these fractures are shown in Figure 4. The two metabasic dykes
747 S3.1. and S3.2, and the brittle fracture zone between the shear zone is referred to as S3 fault
748 zone.



749 The majority of brittle fractures within and outside the S3 shear zone are oriented parallel to
750 the boundaries of the sheared metabasic dykes which strike E-W in the test volume. Very few
751 fractures penetrate into the dykes. Several quartz veins are present with strikes of NNE to E
752 and widths ranging from millimetres up to 30 cm. However, the lateral extension of these
753 quartz veins is limited to the meter range.

754

755 3.2.1.2 Rock mass instrumentation

756 In addition to a detailed characterization of the test volume for the design and interpretation of
757 the in-situ experiment, a dense sensor network is required to collect the necessary data at a
758 sufficient spatial resolution that are needed to address the previously mentioned nine research
759 questions (i.e. research question [1 to 9]). This includes: pore pressure monitoring [research
760 questions 1, 2, 6], strain and tilt [research questions 1, 3, 4, 5, 6] and micro-seismic
761 monitoring [research questions 4, 5, 7, 8, 9]. A major aspect governing the detailed
762 instrumentation design is the type of hydraulic injection treatment (i.e. hydraulic fracturing or
763 hydraulic shearing). For the ISC experiment both hydraulic fracturing (i.e. initiation and
764 propagation of new fractures) and hydraulic shearing (i.e. pressurization of natural structures
765 such as faults) are considered.

766

767 *Pore pressure, deformations and temperature*

768 Four boreholes (three PRP boreholes and SBH15.004; Figure 3) are dedicated to the
769 measurement of the pressure propagation [research questions 1, 2, 6] at points where they cut
770 structures within the test volume during stimulation. These boreholes are completed with
771 resin-grouted packer systems with fixed open intervals of few litres volume for pressure
772 monitoring. The boreholes are drilled approximately normal to the strike of the main
773 geological features. The intervals are chosen to capture the pore pressure within fracture
774 zones or fault zones. Pressure was also recorded in the INJ borehole that was not being
775 injected in the test (Figure 3) by deploying a straddle packer system similar to the one used
776 for high pressure fluid injections. Pore pressure was monitored using a sampling rate of 20
777 Hz. The PRP boreholes were also equipped with pre-stressed distributed fibre optics (FO)
778 cables for strain and temperature measurements. Strain recordings will give information on
779 the HM response to pressurization across pre-existing fractures (e.g. research question 3 and
780 9), as well as on propagation of new fractures during hydrofracturing experiment (e.g.



781 research question 6). Distributed temperature measurements are important for pre- and post-
782 stimulation thermal tracer tests.

783 Additional three boreholes (FBS16.001-3 in Figure 3) are dedicated to the measurement of
784 rock mass deformation associated with hydraulic stimulation. The holes are equipped with
785 both distributed and Fiber Bragg Grating (FBG) strain-sensing optical fibers that are grouted
786 in place. One borehole (FBS16.001) is approximately normal to the strike of the main
787 geological features (i.e. mean strike of the S3 and S1 fault zones, Figure 4) and thus intersects
788 them. One is parallel to the strike of the S3.1 fault and intersects the S1.1 fault (FBS16.002),
789 and one is parallel to the S1.2 faults and intersects the S3 fault zone (FBS16.003). Axial
790 strains developed across sections of the boreholes that span potentially active fractures or the
791 ‘intact’ rock mass between them are measured with FBG sensors that have an operating range
792 of -1000 to 2000 $\mu\epsilon$ and a resolution of 0.1 $\mu\epsilon$. The objective to measure strain parallel to
793 fault zones is to capture the strain field that is associated with fault shearing during
794 stimulation. Strain sensors across structures allow quantifying the fracture dislocation.
795 Distributed strain-sensing optical fibers allow a dense spatial coverage and thus increase the
796 likelihood to observe the propagation direction and opening of a hydraulic fracture. A parallel
797 distribution of untensioned Bragg Grating sensors is used to correct the strains for
798 temperature. All FBG sensors are monitored with a 16 channel si255 Hyperion FBG
799 interrogator (Micronoptics), which is able to record strain or relative temperature from more
800 than 10 sensors per channel with sampling rates of up to 1000 Hz. By averaging up to 1000
801 samples the strain resolution can be improved to $<0.1 \mu\epsilon$. All three FO boreholes are also
802 equipped with a distributed pre-stressed fiber optics cable for strain and temperature
803 monitoring that are recorded with a DiTest device from ominsense.

804 The borehole strain monitoring system is complemented with an array of 3 biaxial tiltmeters
805 installed on the margins of the test volume along the VE tunnel near the S3 fault zone (Figure
806 3). They are mounted in shallow holes drilled into the tunnel floor. The tilt sensors are of type
807 711-2 from Applied Geomechanics, and have a resolution of 0.1 μ radians. Together, the tilt
808 measurements and the longitudinal strain in the FO boreholes will describe the deformation
809 field around the stimulated rock volume and allow constraining the characteristics of the
810 stimulated fault zone (i.e. dimension, dislocation direction and magnitude, etc.), which helps
811 answering research questions 3, 4, 5, and 9.

812

813 *Micro seismicity*

814 Microseismicity is monitored using 14 piezo sensors (Type GMuG Ma-Bls-7-70) affixed to
815 the tunnel walls, and 8 sensors (type GMUG Ma-Bls-7-70) were pressed pneumatically
816 against the borehole wall in the geophysical monitoring boreholes (GEO16.001 – 4, Figure 3
817 and 6). The distribution of sensors within and about the experimental volume ensures optimal
818 azimuthal and vertical coverage around the stimulation points. The uncalibrated piezo sensors
819 are complemented with calibrated accelerometers (Type Wilcoxon 736T) at five locations on
820 the tunnel surface to enable the calculation of absolute magnitudes. The piezo sensors are
821 sensitive to strain signals in the range of 1-100 kHz, while the accelerometers are sensitive
822 from 50 Hz to 40 kHz. Signals from all sensors were recorded continuously on a 32-channel
823 acquisition system (provided by Gesellschaft für Materialprüfung und Geophysik, GMuG) at
824 a sampling rate of 1 MHz. An event detection algorithm with automatic picking of first
825 arrivals allows real time computation of provisional event hypocentres. More detailed
826 processing of the complete data is performed after the experiment (Gischig et al., 2017).
827 Recorded induced seismicity is the basis to answer research question 5, 7 and 8.

828 The sensor network is also used to recorded periodic active seismic experiments. Highly
829 reproducible sources (i.e. piezoelectric pulse sources in boreholes and hammers installed at
830 the tunnel walls with pre-defined constant fall height, Figure 6) are triggered roughly every 10
831 minutes during the stimulation experiments with the goal of recording systematic changes in
832 the waveform characteristics that allow inferring changes of seismic velocity, attenuation and
833 scattering properties. Such measurements can give additional constraints on 3D pressure
834 propagation and deformation characteristics (research question 1 – 4 and 9).

835

836 3.3 Stimulation Phase

837 As both hydroshearing and hydrofracturing are part of above research questions, the
838 stimulation experiments consist of two parts: 1) high-pressure water injection into existing
839 faults or fracture zones within the test volume so that the effective normal stress on the
840 structures is reduced and hydraulic shearing is triggered, and 2) high pressure injection into
841 fracture-free borehole intervals so as to initiate and propagate hydraulic fractures.

842 Two 146 mm diameter, downwardly-inclined boreholes (INJ 1 and INJ 2 in Figure 3) are
843 dedicated for the hydraulic shearing and hydraulic fracturing stimulation injections from
844 packer-isolated intervals. For the stimulation operations, water or gel is injected into a 1-2 m
845 interval in one borehole, and the second borehole is used to monitor the fluid pressure



846 response, together with other dedicated pressure monitoring boreholes. The maximum
847 injected volume for the stimulation at each interval is limited to about 1000 liters, in order to
848 minimize the likelihood of inducing seismic events that could be felt in the tunnels, as well as
849 avoid disturbance to on-going experiments elsewhere in the GTS.

850

851 3.3.1 Hydroshearing experiment

852 The stimulation injections target natural fracture zones in the rock volume whose
853 transmissivities ranges from $1e-8$ to $1e-11$ m²/s. Each interval stimulation consists of three
854 cycles (Figure 7). The objective of the first cycle is to measure initial transmissivity and
855 jacking pressure, and break down the interval. Initially (Cycle 1.1), pressure needs to be
856 increased in small steps until breakdown occurs, as evidenced by a disproportionate increase
857 in flow rate. This first sub-cycle allows to quantify the initial injectivity. After venting, the
858 test needs to be repeated with refined pressure steps (Cycle 1.2) in a narrow range to identify
859 the jacking pressure. After Cycle 1.2 the interval is shut-in to capture the pressure decline
860 curve before the interval is vented. The purpose of the second cycle is to increase the extent of
861 the stimulation away from the injection interval. For this purpose, a step-rate injection test
862 with four steps is utilized with a maximum rate of 37 l/min. The interval is then shut-in and
863 the pressure decline is monitored for 40 minutes before initiating venting for 30 minutes. The
864 purpose of the third cycle is to determine post-stimulation interval transmissivity and jacking
865 pressure for comparison with pre-stimulation values. Thus, a step-pressure test is conducted
866 initially taking small pressure steps to define the low pressure Darcy trend and the deviation
867 from it that occurs at the jacking pressure. Following this cycle, the interval is shut-in for 10
868 minutes before venting. An important aspect for the quantification of irreversible changes in
869 the reservoir is to run acoustic televiewer logs across each interval before and after the
870 stimulation to attempt to resolve any dislocation that may occur across the fractures in the
871 interval.

872

873 3.3.2 Hydraulic fracturing experiment

874 The protocol for hydraulic fracturing tests in borehole intervals without natural fractures are
875 shown in Figure 8. Again, each interval stimulation consists of three cycles. First, the packed
876 interval is tested with a pulse for integrity. The measured transmissivity in intact rock ranges
877 from $1e-13$ to $1e-14$ m²/s. The objective of the first cycle is to break down the formation (i.e.



878 to initiate a hydraulic fracture) using small flow rates (i.e. 5 l/min injections for 60 s). The
879 second cycle aims to propagate the hydraulic fracture away from the well bore and connect to
880 the pre-existing fracture network using progressively increasing flow rates (up to 100 l/min).
881 A shut-in and venting period follows. Finally, the purpose of the third cycle is to quantify the
882 final injectivity and jacking pressure using a pressure step injections similar to the pressure
883 step injection considered for cycle 3 in the fault slip experiments. Both pure water and a gel
884 (i.e. a Xanthan-water-salt-mixture with 0.025 weight percent of Xanthan and 0.1 weight
885 percent of salt with a viscosity between 35 and 40 cPs) are used for fracture propagation. If
886 gel is used, cycle 2 is extended with a flushing cycle (with water) after fracture propagation.
887 The two injection fluids allow investigating two different propagation regimes (toughness-
888 dominated and viscous-dominated). A specific amount of salt was added to each injection
889 fluid as tracer, to investigate flow paths and dilution effects. Further, a cyclic injection
890 sequence is included into the fracture propagation cycle to test it as an alternative injection
891 protocol as proposed by Zang et al. (2013). They propose that using cyclic injection the same
892 efficiency in fracture propagation can be reached, while the associated micro-seismic event
893 release is limited and fracture branching is enhanced.

894

895 3.4 Post-Stimulation Phase

896 The purpose of this phase is to determine the changes to the hydrology and rock mass
897 properties that occurred as a result of each of the two stimulations phases (i.e. the hydraulic
898 shearing and hydraulic fracturing phases). Accordingly, after each phase, a characterization
899 program was performed. The hydraulic properties of the rock mass were determined using
900 single-hole and cross-hole hydraulic methods. Selected stimulation intervals were isolated
901 with packers and then subjected to a variety of tests including pressure-pulse, constant-rate
902 and constant head injection tests, oscillating pumping tests, and tracer tests using solute dyes,
903 DNA-tagged nanoparticles and heat. In addition, single hole, cross-hole, and cross-tunnel
904 active seismic and GPR measurements were conducted. Repeat geophysical borehole logs
905 were run in both injection boreholes, including focused resistivity, and full-wave sonic.

906

907 4 Summary and Conclusion

908 The review of scientific research results showed that carefully analyzed data from large-scale
909 experiments (i.e. EGS projects) and laboratory scale experiments provide a fundamental
910 understanding of processes that underpin permeability creation and induced seismicity in



911 EGS. The results from large-scale experiments suffer from accessibility and resolution which
912 does not permit to resolve the details of seismo-hydro-mechanical coupled processes
913 associated with the stimulation process. Laboratory scale experiment provide a fundamentally
914 improved understanding of these processes but suffer from scalability and test conditions that
915 may lead to over-simplistic fracture flow and/or hydraulic fracture propagation behavior that
916 is not representative for a heterogeneous reservoir. Intermediate-scale experiments can serve
917 to bridge the gap between the laboratory and the large scale and may enable upscaling of
918 results gained from small scale experiments. However, only few intermediate-scale hydro-
919 shearing and hydro-fracturing experiments have recently been performed in a densely
920 instrumented rock mass and no such measurements have been performed on faults in
921 crystalline basement rocks.

922 We have provided here an overview of the intermediate scale hydroshearing and
923 hydrofracturing experiment (i.e. ISC experiment) is being executed in 2017 in the naturally
924 fractured and faulted crystalline rock mass at the Grimsel Test Site (Switzerland). It is
925 designed to fill some of the key research gaps and thus contribute to a better understanding of
926 seismo-hydro-mechanical processes associated with the creation of Enhanced Geothermal
927 Systems. As this contribution is meant to only provide a literature review and an overview of
928 our ISC experiment at the Grimsel Test Site, several other publications will provide more
929 detailed descriptions and analyses of this intermediate-scale hydroshearing and
930 hydrofracturing experiment.

931

932

933

934

935

936

937

938

939

940

941 5 **References**

- 942 Adams, B.M., T.H. Kuehn, J.M. Bielicki, J.B. Randolph, and M.O. Saar (2014). On the
943 importance of the thermosiphon effect in CPG (CO₂ Plume Geothermal) power systems,
944 Energy, DOI: 10.1016/j.energy.2014.03.032, 69:409-418.
- 945 Adams, B.M., T.H. Kuehn, J.M. Bielicki, J.B. Randolph, M.O. Saar (2015). A Comparison of
946 Electric Power Output of CO₂ Plume Geothermal (CPG) and Brine Geothermal
947 Systems for Varying Reservoir Conditions, Applied Energy, DOI:
948 10.1016/j.apenergy.2014.11.043, 140:365–377.
- 949 Ake J, Mahrer K, O’Connell D, Block L. (2005). Deep-Injection and Closely Monitored
950 Induced Seismicity at Paradox Valley, Colorado. Bulletin of the Seismological Society of
951 America, 95(2), 664–683. doi:10.1785/0120040072
- 952 Amitrano, D., (2012). Variability in the power-law distributions of rupture events, Eur. Phys.
953 J. Spec. Top., 205, 199–215.
- 954 Amitrano, D., and J. Schmittbuhl (2002), Fracture roughness and gouge distribution of a
955 granite shear band, *J. Geophys. Res.*, 107(B12), 2375 doi:10.1029/2002JB001761.
- 956 Asanuma H, Soma N, Kaieda H, Kumano Y, Izumi T, Tezuka K, et al. (2005). Microseismic
957 monitoring of hydraulic stimulation at the Australian HDR project in Cooper Basin. In
958 Proceedings World Geothermal Congress (pp. 24–29).
- 959 Bachmann, C., S. Wiemer, B. P. Goertz-Allmann, J. Woessner (2012). Influence of pore
960 pressure on the size distribution of induced earthquakes, Geophysical Research Letters, 38,
961 L09308.
- 962 Bachmann, C., S. Wiemer, J. Woessner, S. Hainzl (2011). Statistical analysis of the induced
963 Basel 2006 earthquake sequence: Introducing a probability-based monitoring approach for
964 Enhanced Geothermal Systems, Geophys. J. Int.
- 965 Baisch, S., Vörös, R., Rothert, E., Stang, H., Jung, R. Schellschmidt, R., (2010). A numerical
966 model for fluid injection induced seismicity at Soutz-sous-Forêt, Int. J. Rock Mech. Min. Sci.,
967 47, 405–413. Baisch, S., Harjes, H.P. (2003). A model for fluid-injection-induced seismicity at
968 the KTB, Germany. Geophysical Journal International 152, 160–170.
- 969 Baisch, S., R. Vörös, R. Weidler, D. Wyborn (2009). Investigation of fault mechanisms
970 during geothermal reservoir stimulation experiments in the Cooper Basin (Australia), Bull.
971 Seismol. Soc. Am. 99, no. 1, 148–158.



- 972 Baisch, S., R. Weidler, R. Vörös, D. Wyborn, L. DeGraaf (2006). Induced seismicity during
973 the stimulation of a geothermal HFR reservoir in the Cooper Basin (Australia), *Bull. Seismol.*
974 *Soc. Am.* 96, no. 6, 2242–2256.
- 975 Baisch, S., Rothert, E., Stang, H., Vörös, R., Koch, Ch., McMahon, A. (2015). Continued
976 Geothermal Reservoir Stimulation Experiments in the Cooper Basin (Australia). *Bulletin of*
977 *the Seismological Society of America*, Vol. 105, No. 1, pp. 198–209
- 978 Bandis S., A.C. Lumsden, N. R. Barton (1983). Fundamentals of rock joint deformation.
979 *International Journal of Rock Mechanics Mining Sciences & Geomech Abstr.*, 20, 6: 249–
980 268.
- 981 Bao X., Eaton D. W. (2016). Fault activation by hydraulic fracturing in western Canada.
982 *Science* 10.1126/science.aag2583
- 983 Baria, R., and A. S. P. Green (1986), Seismicity induced during a viscous stimulation at the
984 Camborne School of Mines Hot Dry Rock Geothermal Energy project in Cornwall, England,
985 paper presented at 8th Int. Acoustic Emission Symp., Japanese Soc. of NDI, Tokyo, Japan,
986 October.
- 987 Barton C.A., M. D. Zoback, D. Moos (1995). Fluid-flow along potentially active faults in
988 crystalline rock. *Geology*, 23, 8: 683–686
- 989 Barton N., S. Bandis, K. Bakhtar (1985). Strength, deformation and conductivity coupling of
990 rock joints. *Int. J. Rock Mech. Min. Sic. & Geomech. Abstr.* 22, 121-140.
- 991 Barton, C.A., S. Hickman, R. Morin, M.D. Zoback, R. Benoit (1998). Reservoir-scale fracture
992 permeability in the Dixie Valley, Nevada, Geothermal Field, paper 47371 presented at
993 SPE/ISRM Eurock '98, Soc. of Pet. Eng., Trondheim, Norway.
- 994 Barton, N.A., Choubey, V., 1977. The shear strength of rock joints in theory and practice.
995 *Rock Mechanics* 10, 1-34.
- 996 Batchelor, A. S., R. Baria, and K. Hearn (1983), Monitoring the effects of hydraulic
997 stimulation by microseismic event location: a case study, in *58th Ann. Tech. Conf. and*
998 *Exhibition of SPE*, edited, Soc. Petrol. Eng., San Francisco, California.
- 999 Baujard, C., Bruel, D., (2006). Numerical study of the impact of fluid density on the pressure
1000 distribution and stimulated volume in the Soultz HDR reservoir, *Geothermics*, 35, 607–
1001 621. Bennour Z, Ishida T, Nagaya Y, Chen Y, Nara Y, Chen Q, Sekine K, Nagano Y (2015)
1002 Crack extension in hydraulic fracturing of shale cores using viscous oil, water, and liquid



- 1003 carbon dioxide. *Rock Mech Rock Eng* 48(4):1463–1473
- 1004 Biot, M.A. (1941). General theory of
1005 three dimensional consolidation. *Journal of Applied Physics*. 12: 155–164.
- 1006 Blake, K., and N. Davatzes (2011), Crustal stress heterogeneity in the vicinity of COCO
1007 geothermal field, CA., paper presented at 36th Workshop on Geothermal Reservoir
1008 Engineering, Stanford University, Stanford University, Jan31-Feb2.
- 1009 Block L., Wood C., Yeck W., King V. (2015). Induced seismicity constraints on subsurface
1010 geological structure, Paradox Valley, Colorado. *Geophysical Journal International*, 200(2),
1011 1170–1193. doi:10.1093/gji/ggu459
- 1012 Bommer, J.J., Oates, S., Cepeda, J.M., Lindholm, C., Bird, J., Torres, R., Marroquín, G.,
1013 Rivas, J., (2006). Control of hazard due to seismicity induced by a hot fractured rock
1014 geothermal project, *Eng. Geol.*, 83, 287–306.
- 1015 Boroumand N, Eaton D. (2012). Comparing Energy Calculations - Hydraulic Fracturing and
1016 Microseismic Monitoring. Presented at the Geoconvention 2012 - 74th Mtg., EAGE,
1017 Copenhagen, C042.
- 1018 Breede, K., Dzebisashvili, K., Liu, X., and Falcone, G. (2013). A systematic review of
1019 enhanced (or engineered) geothermal systems: past, present and future. *Geothermal Energy*,
1020 1(1):1.
- 1021 Brown, D.W., (2000). A hot dry rock geothermal energy concept utilizing supercritical CO2
1022 instead of water. In: *Proceedings of the Twenty-Fifth Workshop on Geothermal Reservoir
1023 Engineering, Stanford, CA. Stanford University.*
- 1024 Brown, D. W., Duchane, D. V., Heiken, G., and Hriscu, V. T. (2012). *Mining the Earth's heat:
1025 hot dry rock geothermal energy.* Springer Science & Business Media.
- 1026 Bruno M, Nakagawa F. (1991). Pore pressure influence on tensile fracture propagation in
1027 sedimentary rock. *International Journal of Rock Mechanics and Mining Sciences &
1028 Geomechanics Abstracts*, 28(4), 261–273. doi:10.1016/0148-9062(91)90593-b
- 1029 Bungler A, Detournay E, Garagash D, Peirce A, others. (2007). Numerical simulation of
1030 hydraulic fracturing in the viscosity dominated regime. In *SPE Hydraulic Fracturing
1031 Technology Conference.* Society of Petroleum Engineers.
- 1032 Bungler AP, Jeffrey RG, Kear J, Zhang X. (2011). Experimental Investigation of the
1033 Interaction among Closely Spaced Hydraulic Fractures. In *45th US Rock Mechanics /
1034 Geomechanics Symposium* (pp. 11–318+). San Francisco.



- 1034 Buscheck, T.A., J.M. Bielicki, T.A. Edmunds, Y. Hao, Y. Sun, J.B. Randolph, and M.O. Saar
1035 (2016). Multifluid geo-energy systems: Using geologic CO₂ storage for geothermal energy
1036 production and grid-scale energy storage in sedimentary basins, *Geosphere*, DOI:
1037 10.1130/GES01207.1, 12(3):678-696.
- 1038 Byerlee, J. (1978). Friction of rocks. *Pure and applied geophysics*, 116(4-5):615-626.
- 1039 Caine, J. S., Evans, J. P., and Forster, C. B. (1996). Fault zone architecture and permeability
1040 structure. *Geology*, 24(11):1025-1028.
- 1041 Calo et al. (2011) Valentin
- 1042 Catalli, F., M.-A. Meier, S. Wiemer (2013). Coulomb stress changes at the Basel geothermal
1043 site: can the Coulomb model explain induced seismicity in an EGS? *Geophys. Res. Lett.*, 40.
- 1044 Chacón E, Barrera V, Jeffrey R, van As A. (2004). Hydraulic fracturing used to precondition
1045 ore and reduce fragment size for block caving. Presented at the MassMin 2004 Santiago
1046 Chile.
- 1047 Chen, Z., S. P. Narayan, Z. Yang, and S. S. Rahman (2000), An experimental investigation of
1048 hydraulic behaviour of fractures and joints in granitic rock, *Int. J. Rock Mech. & Min. Sci.*, 37,
1049 1061-1071.
- 1050 Chitrala, Y., C. Moreno, C. H. Sondergeld, and C. S. Rai (2010), Microseismic mapping of
1051 laboratory induced hydraulic fractures in anisotropic reservoirs, paper presented at Tight Gas
1052 Completions Conference, Society of Petroleum Engineers.
- 1053 Cornet F. H., Helm J., Poitrenaud H., Etchecopar A. (1997). Seismic and Aseismic Slips
1054 Induced by Large-scale Fluid Injections. *Pure appl. geophys.* 150 (1997) 563–583
- 1055 Cornet F.H., Li L., Hulin J.-P., Ippolito I., Kurowski P. (2003). The hydromechanical
1056 behaviour of a fracture: an in situ experimental case study. *International Journal of Rock
1057 Mechanics & Mining Sciences* 40 (2003) 1257–1270
- 1058 Cornet, F. H., and J. Desroches (1989), The problem of channeling in Hot Dry Rock
1059 reservoirs, paper presented at Camborne School of Mines International Hot Dry Rock
1060 Conference, Robertson Scientific Publishers, Llandudno, UK, Cornwall, UK.
- 1061 Cornet, F. H., and O. Scotti (1993), Analysis of induced seismicity for fault zone
1062 identification, *Int. J. Rock Mech. Min. Sci. & Geomech. Abst.*, 30(7), 789-795.



- 1063 Cornet, F. H., and R. H. Jones (1994), Field evidence on the orientation of forced water flow
1064 with respect to the regional principal stress directions, paper presented at 1st North American
1065 Rock Mechanics Symposium, Balkema, Austin, Texas.
- 1066 Cornet, F.H. (2012). The relationship between seismic and aseismic motions induced by
1067 forced fluid injections. *Hydrogeology Journal* 20: 1463–1466.
- 1068 Das I, Zoback MD. (2011). Long-period, long-duration seismic events during hydraulic
1069 fracture stimulation of a shale gas reservoir. *The Leading Edge*, 30(7), 778–786.
1070 doi:10.1190/1.3609093
- 1071 Davies, R., Foulger, G., Bindley, A., Styles, P. (2013). Induced seismicity and hydraulic
1072 fracturing for the recovery of hydrocarbons, *Marine and Petroleum Geology*, 45, 171-185.
- 1073 Deichmann, N., J. Ernst (2009). Earthquake focal mechanisms of the induced seismicity in
1074 2006 and 2007 below Basel (Switzerland), *Swiss J Geosci*, 102(3), 457-466.
- 1075 Deichmann, N., Kraft, T., Evans, K.F, (2014). Identification of faults activated during the
1076 stimulation of the Basel geothermal project from cluster analysis and focal mechanisms of the
1077 larger magnitude events. *Geothermics*, 52 (2014) 84–97.
- 1078 Derode B., F. Cappa, Y. Guglielmi, J. Rutqvist (2013). Coupled seismo-hydromechanical
1079 monitoring of inelastic effects on injection-induced fracture permeability. *International*
1080 *Journal of Rock Mechanics & Mining Sciences* 61: 266–274
- 1081 Detournay, E. (2016). Mechanics of Hydraulic Fractures. In Davis, SH and Moin, P, (eds),
1082 *Annual Review of Fluid Mechanics*, vol 48, p. 311-339.
- 1083 Dusseault MB, McLennan J, Shu J. (2011). Massive multi-stage hydraulic fracturing for oil
1084 and gas recovery from low mobility reservoirs in China. *Petroleum Drilling Techniques*,
1085 39(3), 6–16.
- 1086 Edwards, B., Kraft, T., Cauzzi, C., Kaestli, P., and Wiemer, S. (2015). Seismic monitoring
1087 and analysis of deep geothermal projects in St Gallen and Basel, Switzerland. *Geophysical*
1088 *Journal International*, 201(2):1020-1037.
- 1089 Ellsworth, W.L. (2013). Injection-induced earthquakes. *Science*, 12, 341, 6142
- 1090 Emmermann R, Lauterjung J. (1997). The German Continental Deep Drilling Program KTB:
1091 Overview and major results. *J. Geophys. Res.*, 102(B8), 18179–18201.
1092 doi:10.1029/96jb03945



- 1093 Esaki T., H. Hojo, T. Kimura, N. Kameda, E. (1991). Shear-Flow Coupling Test on Rock
1094 joints. Proceedings – Seventh International Congress on Rock Mechanics, Vol 1: Rock
1095 Mechanics and Environmental Protection.
- 1096 Esaki, T., Du, S., Mitani, Y., Ikusada, K., Jing, L., (1999). Development of a shear-flow test
1097 apparatus and determination of coupled properties for a single rock joint, *Int. J. Rock Mech.*
1098 *Min. Sci.*, 36, 641–650.
- 1099 Evans K. F., F. H. Cornet, T. Hashida, K. Hayashi, T. Ito, K. Matsuki, T. Wallroth (1999).
1100 Stress and rock mechanics issues of relevance to HDR/HWR engineered geothermal systems:
1101 review of developments during the past 15 years. *Geothermics* 28, 455-474
- 1102 Evans K. F., H. Moriya, H. Niitsuma, R.H. Jones, W.S. Phillips, A. Genter, J. Sausse, R.
1103 Jung, R. Baria (2005a). Microseismicity and permeability enhancement of hydrogeologic
1104 structures during massive fluid injections into granite at 3 km depth at the Soultz HDR site,
1105 *Geophys. J. Int.*, 160, 388–412.
- 1106 Evans K.F. (2005). Permeability creation and damage due to massive fluid injections into
1107 granite at 3.5 km at Soultz: 2. Critical stress and fracture strength, *J. geophys. Res.*, 110.
- 1108 Evans K.F., A. Genter, J. Sausse (2005b). Permeability creation and damage due to massive
1109 fluid injections into granite at 3.5 km at Soultz: 1. Borehole observations. *J. geophys. Res.*,
1110 110, B04203.
- 1111 Evans K.F., F. Wyatt (1984). Water table effects on the measurement of earth strain.
1112 *Tectonophysics*, 108: 323-337
- 1113 Evans K.F., T. Kohl, L. Rybach, R.J. Hopkirk (1992). The effect of fracture normal
1114 compliance on the long-term circulation behaviour of a hot dry rock reservoir: A parameter
1115 study using the new fully coupled code fracture. *Geothermal Resources Council Transactions*,
1116 Vol. 16, 449-456, San Diego, CA
- 1117 Evans, J.P., Forster, C.B., Goddard, J.V. (1997). Permeability of fault-related rocks, and
1118 implications for hydraulic structure of fault zones. *J. Struct. Geol.* 19, 1393–1404.
- 1119 Evans, K. F. (1983), Some examples and implications of observed elastic deformations
1120 associated with the growth of hydraulic fractures in the Earth, paper presented at Workshop
1121 on Hydraulic Fracturing Stress Measurements, National Academy Press, Monterey,
1122 California.
- 1123 Evans, K. F. (1998). Does significant aseismic slip occur on fractures in HDR systems under
1124 stimulation conditions? Proceedings, 4th Int. HDR Forum Strasbourg, September 28-30th.



- 1125 Evans, K. F., and P. Meier (1995), Hydro-jacking and hydrofracturing tests in a fissile schist
1126 in south-west Switzerland: In-situ stress characterisation in difficult rock, paper presented at
1127 2nd Int. Conf. on the Mechanics of Jointed and Faulted Rock, Balkema, Vienna, 10-14 April.
- 1128 Evans, K. F., and S. Sikaneta (2013), Characterisation of natural fractures and stress in the
1129 Basel reservoir from wellbore observations (Module 1), in *GEOTHERM: Geothermal*
1130 *Reservoir Processes: Research towards the creation and sustainable use of Enhanced*
1131 *Geothermal Systems*, edited by K. F. Evans, pp. 9-18, Swiss Federal Office of Energy
1132 Publication No 290900, Bern.
- 1133 Evans, K. F., Zappone, A., Kraft, T., Deichmann, N., and Moia, F. (2012). A survey of the
1134 induced seismic responses to uid injection in geothermal and co 2 reservoirs in Europe.
1135 *Geothermics*, 41: 30-54.
- 1136 Evans, K., Holzhausen, G. (1983). On the development of shallow hydraulic fractures as
1137 viewed through the surface deformation field: Part 2-case histories. *Journal of Petroleum*
1138 *Technology*, 35(02):411-420.
- 1139 Evans, K., Wieland, U., Wiemer, S., Giardini D. (2014). Deep Geothermal Energy R&D
1140 Roadmap for Switzerland, 2014.
- 1141 Evans, K. F. (2014), Reservoir Creation, in *Energy from the Earth - Deep Geothermal as a*
1142 *Resource for the Future?*, edited by S. Hirschberg, S. Wiemer and P. Burgherr, pp. 82-118,
1143 Zentrum für Technologiefolgen-Abschätzung, Bern.
- 1144 Eyre, T. S., and M. van der Baan (2015), Overview of moment-tensor inversion of
1145 microseismic events, *The Leading Edge*, August, 882-888 doi: 10.1190/tle34080882.1.
- 1146 Faulkner D., Jackson, C., Lunn, R., Schlische, R., Shipton, Z., Wibberley, C., Withjack, M.,
1147 (2010). A review of recent developments concerning the structure, mechanics and fluid flow
1148 properties of fault zones. *J. Struct. Geol.* 32, 1557–1575.
- 1149 Faulkner D.R., and E.H. Rutter (2008). Can the maintenance of overpressured fluids in large
1150 strike-slip fault zones explain their apparent weakness? *Geology* 29, no. 6: 503–506.
- 1151 Gale, J. E. (1975). A numerical, field and laboratory study of flow in rocks with deformable
1152 fractures. Ph.D. dissertation, Berkeley, University of California, 255 p.
- 1153 Gale, J. E. (1993). Fracture properties from laboratory and large scale field tests: evidence of
1154 scale effects. *Scale Effects in Rock Masses*. Proc. 2nd Int. Workshop on Scale Effects in Rock
1155 Masses (Edited by Pinto da Cunha A.), Lisbon, pp. 341-352. Balkema, Rotterdam.



- 1156 Garagash, D.I., L.N., Germanovich (2012). Nucleation and arrest of dynamic slip on a
1157 pressurized fault, *J. Geophys. Res.*, 117, B10310.
- 1158 Garapati, N., J.B. Randolph, and M.O. Saar (2015). Brine displacement by CO₂, energy
1159 extraction rates, and lifespan of a CO₂-limited CO₂ Plume Geothermal (CPG) system with a
1160 horizontal production well, *Geothermics*, DOI: [10.1016/j.geothermics.2015.02.005](https://doi.org/10.1016/j.geothermics.2015.02.005), 55:182–
1161 194.
- 1162 Genter A. , Goerke X., Graff J.-J, Cuenot N., Krall G., Schindler M., Ravier G. (2010).
1163 Current Status of the EGS Soutz Geothermal Project (France). Proceedings World
1164 Geothermal Congress 2010, Bali, Indonesia, 25-29 April 2010
- 1165 Gentier, S., D. Hopkins, and J. Riss (2000). Role of fracture geometry in the evolution of flow
1166 paths under stress, in *Dynamics of Fluids in Fractured Rock*, Geophys. Monogr. Ser., vol.
1167 122, edited by B. Faybishenko, P. A. Witherspoon, and S. M. Benson, pp. 169 – 184, AGU,
1168 Washington, D. C.
- 1169 Giardini, D. (2009). Geothermal quake risks must be faced, *Nature*, 462 (7275), 848-849.
- 1170 Gischig, V., G. Preisig (2015), Hydro-fracturing versus hydro-shearing: a critical assessment
1171 of two distinct reservoir stimulation mechanisms, paper presented at International Congress of
1172 Rock Mechanics, ISRM 2015, Montréal, Canada.
- 1173 Gischig, V.S., J. Doetsch, H. Maurer, H. Krietsch, F. Amann, K.F. Evans, M. Nejati, M.R.
1174 Jalali, A. Obermann, B. Valley, S. Wiemer, and D. Giardini (2017). On the link between
1175 stress field and small-scale hydraulic fracture growth in anisotropic rock derived from micro-
1176 seismicity. Submitted to Solid Earth.
- 1177 Gischig, V. S. (2015). Rupture propagation behavior and the largest possible earthquake
1178 induced by fluid injection into deep reservoirs. *Geophysical Research Letters*, 42(18):7420-
1179 7428.
- 1180 Gischig, V. S., Wiemer, S. Alcolea, A. R. (2014). Balancing reservoir creation and seismic
1181 hazard in enhanced geothermal systems. *Geophysical Journal International*. doi:
1182 [10.1093/gji/ggu221](https://doi.org/10.1093/gji/ggu221)
- 1183 Gischig, V.S., Wiemer, S. (2013). A stochastic model for induced seismicity based on non-
1184 linear pressure diffusion and irreversible permeability enhancement, *Geophys. J. Int.*, 194(2),
1185 1229–1249.



- 1186 Goebel, T. H. W., T. W. Becker, D. Schorlemmer, S. Stanchits, C. Sammis, E. Rybacki, G.
1187 Dresen (2012). Identifying fault heterogeneity through mapping spatial anomalies in acoustic
1188 emission statistics, *J. Geophys. Res.*, 117, B03310.
- 1189 Goertz-Allmann, B.P., Wiemer, S. (2013). Geomechanical modeling of induced seismicity
1190 source parameters and implications for seismic hazard assessment, *Geophysics*, 78(1), KS25–
1191 KS39.
- 1192 Goertz-Allmann, B.P., Goertz, A., Wiemer, S. (2011). Stress drop variations of induced
1193 earthquakes at the Basel geothermal site, *Geophys. Res. Lett.* 38(9), L09308.
- 1194 Goodman R. E. (1974). The mechanical properties of joints. Proceedings of the 3rd Int.
1195 Congr. International Society of Rock Mechanics, Denver, Colorado. National Academy of
1196 Sciences, Washington, DC, I, 127–140.
- 1197 Guglielmi Y., F. Cappa, H. Lancon, J. B. Janowczyk, J. Rutqvist, C. F. Tsang, J. S. Y. Wang
1198 (2014). ISRM Suggested Method for Step-Rate Injection Method for Fracture In-Situ
1199 Properties (SIMFIP): Using a 3-Components Borehole Deformation Sensor. *Rock Mech.*
1200 *Rock Eng.* 47: 303–311
- 1201 Guglielmi Y., F. Cappa, J. Rutqvist, C.-F. Tsang, A. Thoraval (2008). Mesoscale
1202 characterization of coupled hydromechanical behavior of a fractured-porous slope in response
1203 to free water-surface movement. *Int. J. Rock. Mech. Min. Sci.* 42: 852–878.
- 1204 Guglielmi, Y., Cappa, F., Avouac, J.-P., Henry, P., and Elsworth, D. (2015). Seismicity
1205 triggered by fluid injection induced aseismic slip. *Science*, 348(6240):1224-1226.
- 1206 Guglielmi, Y., F. Cappa, J. Rutqvist, C.-F. Tsang, and A. Thoraval (2006), Field and
1207 numerical investigations of free-water surface oscillation effects on rock slope
1208 hydromechanical behaviour – consequences for rock slope stability analyses paper presented
1209 at GEOPROC 2006: 2nd International Conference on Coupled Thermo-hydro-
1210 mechanicalchemical
- 1211 Guglielmi, Y.G. and Henry, P. Nussbaum, C. Dick, P. Gout, C. Amann, F. (2015).
1212 Underground Research Laboratories for conducting fault activation experiments in shales.
1213 49th US Rock Mechanics / Geomechanics Symposium held in San Francisco, CA, USA,
1214 ARMA 15-0489
- 1215 Gupta, H. K. (1992), *Reservoir-induced Earthquakes*, 364 pp., Elsevier, Amsterdam, The
1216 Netherlands.



- 1217 Haimson, B. C., and F. H. Cornet (2003), ISRM suggested methods for rock stress estimation-
1218 Part 3: hydraulic fracture (HF) and/or hydraulic testing of pre-existing fractures (HTPF), *Int.*
1219 *J. Rock Mech. Min. Sci.*, *40*, 1011-1020.
- 1220 Hampton, J. C., L. Matzar, D. Hu, and M. Gutierrez (2015), Fracture dimension investigation
1221 of laboratory hydraulic fracture interaction with natural discontinuity using acoustic emission,
1222 paper presented at 49th US Rock Mechanics/Geomechanics Symposium, Americal Rock
1223 Mechanics Association, San Francisco, 28 June-1 July.
- 1224 Häring, M.O., Schanz, U., Ladner, F. & Dyer, B.C., (2008). Characterization of the Basel 1
1225 enhanced geothermal system, *Geothermics*, *37*, 469–495.
- 1226 Healy, J. H., W. W. Rubey, D. T. Griggs, and C. B. Raleigh (1968), The Denver earthquakes,
1227 *Science*, *161*, 1301-1310.
- 1228 Hickman, S. H., M. Zoback, C. A. Barton, R. Benoit, J. Svitek, Summer, and R.
1229 (2000), Stress and permeability heterogeneity within the Dixie Valley geothermal reservoir:
1230 recent results from well 82-5, paper presented at Twenty-Fifth Workshop on Geothermal
1231 Reservoir Engineering, Stanford University, Stanford University, Stanford, CA, Jan 24-26.
- 1232 Hickman, S., M. D. Zoback, and R. Benoit (1998), Tectonic controls on fault-zone
1233 permeability in a geothermal reservoir at Dixie Valley, Nevada, paper 47213 presented at
1234 SPE/ISRM Eurock '98, Soc. of Pet. Eng., Trondheim, Norway.
- 1235 Hogarth, R., H. Holl, and A. McMahon (2013), Flow testing results from Habanero EGS
1236 Project, paper presented at Australian Geothermal Energy Conferences, Brisbane, Australia,
1237 14-15 November.
- 1238 Horálek, J., Z. Jechumtálová, L. Dorbath, and J. Síleny (2010), Source mechanisms of micro-
1239 earthquakes induced in a fluid injection experiment at the HDR site Soultz-sous-Forêts
1240 (Alsace) in 2003 and their temporal and spatial variations, *Geophys. J. Int.*, *181*, 1547-1565
1241 doi: 10.1111/j.1365-246X.2010.04506.x.
- 1242 Houben, G. (2015), Review: Hydraulics of water wells—flow laws and influence of
1243 geometry, *Hydrogeology J.*, *23*, 1633-1657.
- 1244 Hubbert, M. K. and Rubey, W. W. (1959). Role of uid pressure in mechanics of overthrust
1245 faulting i. mechanics of uid-illed porous solids and its application to overthrust faulting.
1246 Geological Society of America Bulletin, *70*(2):115{166.
- 1247 Hummel, N., and T. M. Müller (2009), Microseismic signatures of non-linear pore-fluid
1248 pressure diffusion, *Geophys. J. Int.*, *179*, 1558-1565 doi: 10.1111/j.1365-246X.2009.04373.x.



- 1249 Husen, S., C. Bachmann, D. Giardini (2007). Locally triggered seismicity in the central
1250 Swiss Alps following the large rainfall event of August 2005. *Geophysical Journal*
1251 *International*, 171 (2007), pp. 1126-1134, 10.1111/j.1365-246X.2007.03561.x
- 1252 Huw, C., Eisner, L., Styles, P., Turner, P., (2014). Felt seismicity associated with shale gas
1253 hydraulic fracturing: The first documented example in Europe, *Geophysical Research Letter*,
1254 doi: 10.1002/2014GL062047
- 1255 Ishida T. (2001). Acoustic emission monitoring of hydraulic fracturing in laboratory and field.
1256 *Construction and Building Materials* 15 Ž2001. 283-295
- 1257 Jaeger JC. (1963). Extension Failures in Rocks subject to fluid Pressure. *Journal of*
1258 *Geophysical Research*, 68(21), 6066–6067.
- 1259 Jeanne, P., Y. Guglielmi, and F. Cappa. 2012. Dissimilar properties within a carbonate-
1260 reservoir’s small fault zone, and their impact on the pressurization and leakage associated
1261 with CO₂ injection. *Journal of Structural Geology*. DOI:10.1016/j.jsg.2012.10.010
- 1262 Jeffrey R, Enever J, Phillips R, Ferguson T, Davidson S, Bride J. (1993). Small-Scale
1263 Hydraulic Fracturing and Mineback Experiment in Coal Seams. Presented at the Proceedings
1264 of the 1993 International Coalbed methane Symposium.
- 1265 Jeffrey RG, Brynes RP, Lynch PJ, Ling DJ. (1992). An Analysis of Hydraulic Fracture and
1266 Mineback Data for a Treatment in the German Creek Coal Seam. *Society of Petroleum*
1267 *Engineers*. doi:10.2118/24362-MS
- 1268 Jeffrey RG, Bungler A. (2007). A Detailed Comparison of Experimental and Numerical Data
1269 on Hydraulic Fracture Height Growth Through Stress Contrasts. *Society of Petroleum*
1270 *Engineers*. doi:10.2118/106030-MS
- 1271 Jeffrey RG, Bungler AP, Lecampion B, Zhang X, Chen ZR, van As A, et al. (2009).
1272 Measuring Hydraulic Fracture Growth in Naturally Fractured Rock. In 2009 SPE Annual
1273 Technical Conference and Exhibition (p. SPE 124919+). New Orleans, Louisiana, USA: SPE.
- 1274 Jeffrey RG, Settari A. (1995). A Comparison of Hydraulic Fracture Field Experiments,
1275 Including Mineback Geometry Data, with Numerical Fracture Model Simulations. *Society of*
1276 *Petroleum Engineers*. doi:10.2118/30508-MS
- 1277 Johnson E, Cleary MP. (1991). Implications of recent laboratory experimental results for
1278 hydraulic fractures. *Society of Petroleum Engineers*. doi:10.2118/21846-MS



- 1279 Jost M, Bübelberg T, Jost Ö, Harjes H. (1998). Source parameters of injection-induced
1280 microearthquakes at 9 km depth at the KTB Deep Drilling site, Germany. *Bulletin of the*
1281 *Seismological Society of America*, 88(3), 815–832.
- 1282 Jung R. (1989). Hydraulic in situ investigations of an artificial fracture in the Falkenberg
1283 Granite. *Int. J. Rock Mech. Min. Sci. & Geomech. Abstr.* 26: 301-308.
- 1284 Jung R. (2013). EGS — Goodbye or Back to the Future. *Effective and Sustainable Hydraulic*
1285 *Fracturing*, <http://dx.doi.org/10.5772/56458>
- 1286 Jupe A. Green A. S. P., Wallroth T. (1992). Induced Microseismicity and Reservoir Growth at
1287 the Fjällbacka Hot Dry Rocks Project, Sweden. *Int. J. Rock Mech. Min. Sci. & Geomech.*
1288 *Abstr. Vol. 29. No. 4. pp. 343-354.*
- 1289 Kaieda, H., Jones, R., Moriya, H., Sasaki, S. & Ushijima, K., (2005). Ogachi HDR reservoir
1290 evaluation by AE and geophysical methods, in *Proceedings of World Geothermal Congress*
1291 *2005, Antalya, Turkey, April 24–29.*
- 1292 Karvounis, D.C., Gischig, V.S., Wiemer, S., (2014). Towards a Real-Time Forecast of
1293 Induced Seismicity for Enhanced Geothermal Systems. *Proceedings of the 2014 Shale Energy*
1294 *Engineering Conference, July 21–23, 2014, Pittsburgh, Pennsylvania, 246.*
- 1295 Keranen, K., M, Savage, H. M., Abers, G. A., & Cochran, E. S. (2013). Potentially induced
1296 earthquakes in Oklahoma, USA: Links between wastewater injection and the 2011 Mw 5.7
1297 earthquake sequence, *Geology* 41 (6), 699–702, doi:10.1130/G34045.1
- 1298 Keusen, H.R., Ganguin, J., Schuler, P., Buletti, M., 1989. Grimsel test site: *Geology.*
1299 *Nationale Genossenschaft fuer die Lagerung Radioaktiver Abfaelle (NAGRA), Baden,*
1300 *Switzerland. Technical Report NTB 87-14E, 166 pp.*
- 1301 Király, E., Zechar, J.D., Gischig, V.S, Karvounis, D., Doetsch, J., Wiemer, S., (2015).
1302 *Modeling Induced Seismicity and Validating Models in Deep Geothermal Energy Projects.* In
1303 *preparation.*
- 1304 Kohl, T., K. F. Evans, R. J. Hopkirk, R. Jung, and L. Rybach (1997), Observation and
1305 simulation of non-Darcian flow transients in fractured rock, *Wat. Resourc. Res.*, 33(3), 407-
1306 418.
- 1307 Krietsch, H., V. Gischig, R. Jalali, F. Amann, K. F. Evans, J. Doetsch, and B. Valley (2017),
1308 *Stress measurements in crystalline rock: Comparison of overcoring, hydraulic fracturing and*
1309 *induced seismicity results, in ARMA 51st US Rock Mechanics / Geomechanics Symposium,*
1310 *edited, San Francisco, California, USA.*



- 1311 Lee, H. S., and T. F. Cho (2002), Hydraulic Characteristics of Rough Fractures in Linear
1312 Flow under Normal and Shear Load, *Rock Mech. Rock Eng.*, 35, 299-318 DOI
1313 10.1007/s00603-002-0028-y.
- 1314 Lee, H.S., Cho, T.F. (2002). Hydraulic characteristics of rough fractures in linear flow under
1315 normal and shear load, *Rock Mech. Rock Eng.*, 35(4), 299–318.
- 1316 Louis, C., J.-L., Dessene, B. Feuga (1977). Interaction between water flow phenomena and
1317 the mechanical behavior of soil or rock masses. Gudehns, G., ed., *Finite elements in*
1318 *geomechanics*: New York, John Wiley S Sons, 572 p.
- 1319 Majer, E., J. Nelson, A. Robertson-Tait, J. Savy, and I. Wong (2012). Protocol for addressing
1320 induced seismicity associated with enhanced geothermal systems, U.S. Department of
1321 Energy, Energy Efficiency and Renewable Energy.
- 1322 Manning, C. and Ingebritsen, S. (1999). Permeability of the continental crust: Implications of
1323 geothermal data and metamorphic systems. *Reviews of Geophysics*, 37(1):127/150.
- 1324 Marone, C., and C. H. Scholz (1988), The depth of seismic faulting and the upper transition
1325 from stable to unstable slip regimes, *Geophys. Res. Lett.*, 15(6), 621-624 DOI:
1326 10.1029/GL015i006p00621.
- 1327 Martin C. D., C. C. Davison, E. T. Kozak (1990). Characterizing normal stiffness and
1328 hydraulic conductivity of a major shear zone in granite. *Rock joints*, eds. Barton &
1329 Stephansson, Balkema, Rotterdam, Netherlands.
- 1330 Maury, V., 1994. Rock failure mechanisms identification: A key for wellbore stability and
1331 reservoir behaviour problem, in *Eurock 94*, edited by Delft, Netherlands, 29-31 August, 175-
1332 182, Balkema.
- 1333 Maxwell, S. (2014), *Microseismic Imaging of Hydraulic Fracturing: Improved Engineering of*
1334 *Unconventional Shale Reservoirs*, 197 pp., Society of Exploration Geophysicists.
- 1335 McClure, M. W. (2015), Generation of large postinjection-induced seismic events by
1336 backflow from dead-end faults and fractures, *Geophysical Research Letters*, 42(6647–6654).
- 1337 McClure M.W., R. N. Horne (2011). Investigation of injection-induced seismicity using a
1338 coupled fluid flow and rate/state friction model. *Geophysics* 76, 6.
- 1339 McClure M.W., R. N. Horne (2014). An investigation of stimulation mechanisms in
1340 Enhanced Geothermal Systems *International Journal of Rock Mechanics & Mining Sciences*
1341 72: 242–260



- 1342 McClure, M. W. (2012). Modeling and characterization of hydraulic stimulation and induced
1343 seismicity in geothermal and shale gas reservoirs. PhD thesis, Stanford University.
- 1344 McGarr, A. (1976). Seismic moments and volume changes, *Journal of Geophysical Research*,
1345 81(8), 1487-1494.
- 1346 Mena, B., Wiemer, S., Bachmann, C., (2013). Building robust model to forecast the induced
1347 seismicity related to geothermal reservoir enhancements, *Bull. seism. Soc. Am.*, 103(1), 383–
1348 393.
- 1349 Meng, C. (2011), Hydraulic fracture propagation in pre-fractured rocks, paper presented at
1350 SPE Hydraulic Fracturing Technology Conference and Exhibition, SPE, The Woodlands,
1351 Texas, 24-26 Jan.
- 1352 Mignan, A., Landtwing, D., Kästli, P., Mena, B., Wiemer, S. (2015). Induced seismicity risk
1353 analysis of the 2006 Basel, Switzerland, Enhanced Geothermal System project: Influence of
1354 uncertainties on risk mitigation, *Geothermics*, 53 (2015) 133–146.
- 1355 Murdoch LC, Schweisinger T, Svenson E, Germanovich L. (2004). Measuring and analyzing
1356 transient changes in fracture aperture during well tests: preliminary results. In: *Dynamics of*
1357 *fluids in fractured rock (Witherspoon Conference)*. LBL Report 54275, February 10–14,
1358 2004. p. 129–32.
- 1359 Murphy H., C. Huang, Z. Dash, G. Zyvoloski, A. White (2004). Semi-analytical solutions for
1360 fluid flow in rock joints with pressure-dependent openings. *Water Resources Research* 40,
1361 W12506
- 1362 Nicholson, C., and R. L. Wesson (1990), Earthquake Hazard Associated with Deep Well
1363 Injection-A Report to the U.S. Environmental Protection Agency, 1951, US Geological
1364 Survey Bulletin.
- 1365 Nicol, D. A. C., and B. A. Robinson (1990), Modelling the heat extraction from the
1366 Rosemanowes HDR reservoir, *Geothermics*, 19, 247-257.
- 1367 Niitsuma H., M. Fehler, R. Jones, S. Wilson, J. Albright, A. Green, R. Baria, K. Hayashi, H.
1368 Kaieda, K. Tezuka, A. Jupe, T. Wallroth, F. Cornet, H. Asanuma, H. Moriya, K. Nagano,
1369 W.S. Phillips, J. Rutledge, L. House, A. Beauce, D. Alde, R. Aster (1999). Current status of
1370 seismic and borehole measurements for HDR/HWR development. *Geothermics*, 28, 4-5: 475-
1371 490.



- 1372 Olsson R., N. Barton (2001). An improved model for hydromechanical coupling during
1373 shearing of rock joints. *International Journal of Rock Mechanics and Mining Sciences*, 38, 3:
1374 317–329.
- 1375 Parker R. (1999). The Rosemanowes HDR project 1983-1991. *Geothermics*, 28, 603-615.
- 1376 Parker, R. H. (1989a), Hot Dry Rock Geothermal Energy: Phase 2B Final Report of the
1377 Camborne School of Mines Project, 1391 pp., Pergamon Press, Oxford.
- 1378 Pearson, C. (1981), The relationship between microseismicity and high pore pressures during
1379 hydraulic stimulation experiments in low porosity granitic rock, *J. Geophys. Res.*, 86, 7855-
1380 7864.
- 1381 Pettitt W, Pierce M, Damjanac B, Hazzard J, Lorig L, Fairhurst C, et al. (2011). Fracture
1382 network engineering for hydraulic fracturing. *The Leading Edge*, 30(8), 844–853.
1383 doi:10.1190/1.3626490
- 1384 Petty, S., Nordin, Y., Glassely, W., Cladouhos, T. (2013). Improving geothermal project
1385 economics with multi-zone stimulation: results from the Newberry volcano EGS
1386 demonstration. Proc. 38th Works. Geoth. Rese. Eng., Stanford University, SGP-TR-198.
- 1387 Phillips, S., L. S. House, and M. C. Fehler (1997), Detailed joint structure in a geothermal
1388 reservoir from studies of induced microseismic clusters, *J. Geophys. Res.*, 102(B6), 11,745-
1389 711,763.
- 1390 Pine, R.J., Baria, R., Pearson, R.A., Kwakwa, K., McCartney, R (1987). A Technical
1391 Summary of Phase 2B of the Camborne School of Mines HDR Project, 1983-1986.
1392 *Geothermics*, 16, 4: 341-353.
- 1393 Potter, R., Robinson, E., and Smith, M. (1974). Method of extracting heat from dry
1394 geothermal reservoirs. US Patent 3,786,858.
- 1395 Power, W. L., and T. E. Tullis (1991), Euclidean and fractal models for the description of
1396 surface roughness, *J. Geophys. Res.*, 96(B1), 415-424.
- 1397 Preisig, G., E. Eberhardt, V. Gischig, V. Roche, M. Van der Baan, B. Valley, P. Kaiser, and
1398 D. Du (2015), Development of connected rock mass permeability by hydraulic fractures
1399 growth accompanying fluid injection, *Geofluids* 15, 321–337. Rahman, M.K., Hossain, M.M.,
1400 Rahman, S.S. (2002). A shear-dilation-based model for evaluation of hydraulically stimulated
1401 naturally fractured reservoirs. *International Journal for Numerical and Analytical Methods in*
1402 *Geomechanics*, 26, 5: 469-497.



- 1403 Pruess, K., (2006). Enhanced geothermal systems (EGS) using CO₂ as working fluid – a
1404 novel approach for generating renewable energy with simultaneous sequestration of carbon.
1405 *Geothermics* 35 (4), 351–367.
- 1406 Pruess, K., (2007). Role of fluid pressure in the production behavior of enhanced geothermal
1407 systems with CO₂ as working fluid. *GRC Trans.* 31, 307–311.
- 1408 Raleigh, C., Healy, J., and Bredehoeft, J. (1976). An experiment in earthquake control at
1409 Rangely, Colorado. *work (Fig. 1b)*, 108(52):30.
- 1410 Randolph, J.B., and M.O. Saar (2011a), Combining geothermal energy capture with geologic
1411 carbon dioxide sequestration, *Geophysical Research Letters*, DOI: 10.1029/2011GL047265,
1412 38, L10401.
- 1413 Randolph, J.B. and M.O. Saar (2011b). Coupling carbon dioxide sequestration with
1414 geothermal energy capture in naturally permeable, porous geologic formations: Implications
1415 for CO₂ sequestration, *Energy Procedia*, DOI: 10.1016/j.egypro.2011.02.108, 4:2206-2213.
- 1416 Rutledge, J. T., Phillips, W. S., & Mayerhofer, M. J.: Faulting Induced by Forced Fluid
1417 Injection and Fluid Flow Forced by Faulting: An Interpretation of Hydraulic-Fracture
1418 Microseismicity, Carthage Cotton Valley Gas Field, Texas, *Bulletin of the Seismological*
1419 *Society of America*, 94, (2004),1817.
- 1420 Rutqvist J. (1995): Determination of hydraulic normal stiffness of fractures in hard rock from
1421 well testing. *Int. J. Rock Mech. Min. Sci.*, 32: 513–23.
- 1422 Rutqvist J., O. Stephansson (2003). The role of hydromechanical coupling in fractured rock
1423 engineering. *Hydrogeology Journal*, 11, 1:7–40.
- 1424 Rutqvist, J. (2011). Status of the tough-ac simulator and recent applications related to coupled
1425 fluid flow and crustal deformations. *Computers & Geosciences*, 37(6):739-750.
- 1426 Rutqvist, J., and C. M. Oldenburg (2008), Analysis of injection-induced micro-earthquakes in
1427 a geothermal steam reservoir, Geysers Geothermal Field, California, *Proceedings of the 42th*
1428 *U. S. Rock Mechanics Symposium*, June 29–July 2, 2008, San Francisco, California, USA,
1429 151.
- 1430 Rutqvist, J., and O. Stephansson (1996), A cyclic hydraulic jacking test to determine the in-
1431 situ stress normal to a fracture, *Int. J. Rock Mech. Min. Sci. & Geomech. Abstr.*, 33(7), 695-
1432 711.



- 1433 Saar, M.O., and M. Manga (2003). Seismicity induced by seasonal groundwater recharge at
1434 Mt. Hood, Oregon, Earth and Planetary Science Letters, DOI: 10.1016/S0012-
1435 821X(03)00418-7, 214:605-618.
- 1436 Saar, M.O., and M. Manga (2004). Depth dependence of permeability in the Oregon Cascades
1437 inferred from hydrogeologic, thermal, seismic, and magmatic modeling constraints, Journal
1438 of Geophysical Research, DOI: 10.1029/2003JB002855, 109, Nr. B4, B04204.
- 1439 Saar, M.O. (2011). Review: Geothermal heat as a tracer of large-scale groundwater flow and
1440 as a means to determine permeability fields, Hydrogeology Journal, DOI: 10.1007/s10040-
1441 010-0657-2, 19:31-52, 2011.
- 1442 Saar, M.O. (to be published 2017). Novel Geothermal Technologies, in Potentials, costs and
1443 environmental assessment of electricity generation technologies, edited by C. Bauer and S.
1444 Hirschberg, Swiss Federal Office of Energy, Swiss Competences Center for Energy Research
1445 "Supply of Electricity", Swiss Competence Center for Energy Research "Biomass for Swiss
1446 Energy Future".
- 1447 Schanz U, Dyer B, Ladner F, Haering MO. (2007). Microseismic aspects of the Basel 1
1448 geothermal reservoir. In 5th Swiss Geoscience Meeting. Geneva.
- 1449 Schmittbuhl, J., F. Schmitt, and C. H. Scholz (1995), Scaling invariance of crack surfaces, *J.*
1450 *Geophys. Res.*, 100(B4), 5953-5973.
- 1451 Schoenball, M., Baujard, C., Kohl, T., Dorbath, L. (2012). The role of triggering by static
1452 stress transfer during geothermal reservoir stimulation, *J. geophys. Res.*, 117, B09307.
- 1453 Scholz, C. H. (2015), On the stress dependence of the earthquake b value, *Geophys. Res. Lett.*,
1454 42, 1399-1402 doi:10.1002/2014GL062863.
- 1455 Scholz, C.H., 1990. The mechanics of Earthquakes and Faulting. Cambridge University Press,
1456 Cambridge, UK, p. 39.
- 1457 Schorlemmer, D., S. Wiemer, Wyss, M., (2005). Variations in earthquake size distribution
1458 across different stress regimes, *Nature*, 437, 539–542.
- 1459 Schrauf T. W., Evans D. D. (1986). Laboratory Studies of Gas Flow Through a Single Natural
1460 Fracture WATER RESOURCES RESEARCH, VOL. 22, NO. 7, 1038-1050
- 1461 Schweisinger T., E.J. Swenson, L.C. Murdoch (2009): Introduction to hydromechanical well
1462 tests in fractured rock aquifers. *Groundwater* 47, 1:69–79



- 1463 Schweisinger, T., L.C. Murdoch, and C.O. Huey Jr. (2007). Design of a removable borehole
1464 extensometer. *Geotechnical Testing Journal* 30, no. 3: 202–211.
- 1465 Scotti O., Cornet F.H. (1994). In situ evidence for fluid induced aseismic slip events along
1466 fault zones. *Int J Rock Mech Min* 1:347-358.
- 1467 Shamir, G., and M. D. Zoback (1992), Stress orientation profile to 3.5 km depth near the San
1468 Andreas fault at Cajon Pass, California, *J. Geophys. Res.*, 97, 5059-5080.
- 1469 Sileny, J., D. P. Hill, and F. H. Cornet (2009), Non–double-couple mechanisms of
1470 microearthquakes induced by hydraulic fracturing, *J. Geophys. Res.*, 114, B08307
1471 doi:10.1029/2008JB005987.
- 1472 Song I, Suh M, Won K, Haimson B. (2001). A laboratory study of hydraulic fracturing
1473 breakdown pressure in tablerock sandstone. *Geosciences Journal*, 5(3), 263–271.
1474 doi:10.1007/bf02910309
- 1475 Spada, M., Tormann, T., Goebel, T., Wiemer, S. (2013). Generic dependence of the
1476 frequency-size distribution of earthquakes on depth and its relation to the strength profile of
1477 the crust, *Geophys. Res. Lett.*, 40(4), 709–714.
- 1478 Stein, R. S. (1999). The role of stress transfer in earthquake occurrence. *Nature*, 402(6762):
1479 605-609.
- 1480 Tenma N., Yamaguchi T., Zylvoski G. (2008). The Hijiori Hot Dry Rock test site, Japan
1481 evaluation and optimization of heat extraction from a two-layered reservoir. *Geothermics*
1482 2008; 37:19–52.
- 1483 Terakawa, T., Miller, S.A., Deichmann, N. (2012). High fluid pressure and triggered
1484 earthquakes in the enhanced geothermal system in Basel, Switzerland, *J. Geophys. Res.*, 117,
1485 B07305.
- 1486 Tester, J. W., Anderson, B. J., Batchelor, A., Blackwell, D., DiPippo, R., Drake, E.,
1487 Garnish, J., Livesay, B., Moore, M., Nichols, K., et al. (2006). The future of geothermal
1488 energy. *Impact of Enhanced Geothermal Systems (EGS) on the United States in the 21st*
1489 *Century*, Massachusetts Institute of Technology, Cambridge, MA, page 372.
- 1490 Tezuka, K., and H. Niitsuma (2000), Stress estimated using microseismic clusters and its
1491 relationship to the fracture system of the Hijiori Hot Dry Rock reservoir, *Engineering*
1492 *Geology*, 56, 47-62.



- 1493 Tormann, T., B Enescu, J. Woessner and S. Wiemer (2015). Randomness of megathrust
1494 earthquakes implied by rapid stress recovery after the Japan earthquake, *Nature Geoscience* 8
1495 (2), 152-158.
- 1496 Tormann, T., S. Wiemer, A. Mignan (2014). Systematic survey of high-resolution b value
1497 imaging along Californian faults: Inference on asperities, *J. Geophys. Res. Solid Earth*,
1498 119(3), 2029–2054.
- 1499 Valley, B., and K. F. Evans (2009), Stress orientation to 5 km depth in the basement below
1500 Basel (Switzerland) from borehole failure analysis, *Swiss J. Earth Sci.*, 102, 467-480 doi:
1501 10.1007/s00015-009-1335-z.
- 1502 Valley, B., and K. F. Evans (2010), Stress Heterogeneity in the Granite of the Soultz EGS
1503 Reservoir Inferred from Analysis of Wellbore Failure, paper presented at World Geothermal
1504 Congress, International Geothermal Association, Bali, 25-29 April 2010
- 1505 van As A, Jeffrey R. (2002). Hydraulic fracture growth in naturally fractured rock: mine
1506 through mapping and analyses. Presented at the NARMS-TAC conference, Toronto, Canada.
- 1507 van As A, Jeffrey RG. (2000). Caving Induced by Hydraulic Fracturing at Northparkes
1508 Mines. Presented at the 4th North American Rock Mechanics Symposium, American Rock
1509 Mechanics Association. <https://www.onepetro.org/conference-paper/ARMA-2000-0353>.
1510 Accessed 26 September 2015
- 1511 van As, A., Jeffrey R., Chacón E. and Barrera, V. (2004). Preconditioning by hydraulic
1512 fracturing for bloc caving in a moderately stressed naturally fractured orebody. Proceeding of
1513 the Massmin 2004 conference, Santiago Chile, 22-25 August 2004.
- 1514 van der Baan M, Eaton D, Dusseault M. (2013). Microseismic Monitoring Developments in
1515 Hydraulic Fracture Stimulation. In R Jeffrey (Ed.), *Effective and Sustainable Hydraulic*
1516 *Fracturing*. InTech. [http://www.intechopen.com/books/effective-and-sustainable-hydraulic-](http://www.intechopen.com/books/effective-and-sustainable-hydraulic-fracturing/microseismic-monitoring-developments-in-hydraulic-fracture-stimulation)
1517 [fracturing/microseismic-monitoring-developments-in-hydraulic-fracture-stimulation](http://www.intechopen.com/books/effective-and-sustainable-hydraulic-fracturing/microseismic-monitoring-developments-in-hydraulic-fracture-stimulation).
1518 Accessed 25 September 2015
- 1519 Vermylen J, Zoback MD. (2011). Hydraulic Fracturing, Microseismic Magnitudes, and Stress
1520 Evolution in the Barnett Shale, Texas, USA. Society of Petroleum Engineers.
1521 doi:10.2118/140507-MS
- 1522 Vogler D., Amann F., Bayer P., Elsworth D. (2015). Permeability Evolution in Natural
1523 Fractures Subject to Cyclic Loading and Gouge Formation. *RMRE*, 49(9).



- 1524 Warpinski N. (2009). Microseismic Monitoring: Inside and Out. *Journal of Petroleum*
1525 *Technology*, 61(11), 80–85. doi:10.2118/118537-JPT
- 1526 Warpinski N. (2013). Understanding Hydraulic Fracture Growth, Effectiveness, and Safety
1527 Through Microseismic Monitoring. In R Jeffrey (Ed.), *Effective and Sustainable Hydraulic*
1528 *Fracturing*. InTech. [http://www.intechopen.com/books/effective-and-sustainable-hydraulic-](http://www.intechopen.com/books/effective-and-sustainable-hydraulic-fracturing/understanding-hydraulic-fracture-growth-effectiveness-and-safety-through-microseismic-monitoring)
1529 [fracturing/understanding-hydraulic-fracture-growth-effectiveness-and-safety-through-](http://www.intechopen.com/books/effective-and-sustainable-hydraulic-fracturing/understanding-hydraulic-fracture-growth-effectiveness-and-safety-through-microseismic-monitoring)
1530 [microseismic-monitoring](http://www.intechopen.com/books/effective-and-sustainable-hydraulic-fracturing/understanding-hydraulic-fracture-growth-effectiveness-and-safety-through-microseismic-monitoring). Accessed 26 September 2015
- 1531 Warpinski N., L. W. Teufel (1987): Influence of geologic discontinuities on hydraulic fracture
1532 propagation. *J. Petrol. Technol.* 39: 209–20
- 1533 Warpinski NR, Clark JA, Schmidt RA, Huddle CW. (1982). Laboratory Investigation on the -
1534 Effect of In-Situ Stresses on Hydraulic Fracture Containment. *Society of Petroleum Engineers*
1535 *Journal*, 22(03), 333–340. doi:10.2118/9834-PA
- 1536 Warpinski NR, Du J. (2010). Source-Mechanism Studies on Microseismicity Induced by
1537 Hydraulic Fracturing. *Society of Petroleum Engineers*. doi:10.2118/135254-MS
- 1538 Warpinski NR. (1985). Measurement of Width and Pressure in a Propagating Hydraulic
1539 Fracture. *Society of Petroleum Engineers Journal*, 25(01), 46–54. doi:10.2118/11648-PA
- 1540 Warren W. E., Schmith C. W. (1985). In Situ Stress Estimates From Hydraulic Fracturing and
1541 Direct Observation of Crack Orientation. *Journal of Geophysical Research*, Vol. 9, NO. B8,
1542 829-68
- 1543 Wehrens, P. (2015). Structural evolution in the Aar Massif (Haslital transect): Implications
1544 for the mid-crustal deformation. PhD thesis, University Bern.
- 1545 Wolhart, S. L., T. A. Harting, J. E. Dahlem, T. Young, M. J. Mayerhofer, and E. P. Lolon
1546 (2006), Hydraulic fracture diagnostics used to optimize development in the Jonah field., paper
1547 presented at SPE Annual Technical Conference and Exhibition. *Society of Petroleum*
1548 *Engineers*.
- 1549 Yeo I. W., M. H. De Freitas, and R. W. Zimmerman (1998). Effect of shear displacement on
1550 the aperture and permeability of a rock fracture. *International Journal of Rock Mechanics and*
1551 *Mining Sciences*, 35, 8:1051–1070
- 1552 Yoon, J.-S., Zang, A., Stephansson, O., 2014. Numerical investigation on optimized
1553 stimulation of intact and naturally fractured deep geothermal reservoirs using hydro-
1554 mechanical coupled discrete particles joints model. *Geothermics*, 52.



1555 Zang A, Yoon J.S., Stephansson O, Heidbach O. (2013). Fatigue hydraulic fracturing by
1556 cyclic reservoir treatment enhances permeability and reduces induced seismicity. *Geophysical*
1557 *Journal International*, 195(2), 1282–1287. doi:10.1093/gji/ggt301

1558 Zang A., Stephansson O. (2013). *Stress Field of the Earth's Crust*. Springer Dordrecht
1559 Heidelberg London New York, DOI 10.1007/978-1-4020-8444-7.

1560 Ziegler M, Valley B, Evans K. (2015). Characterisation of Natural Fractures and Fracture
1561 Zones of the Basel EGS Reservoir Inferred from Geophysical Logging of the Basel-1 Well.
1562 Presented at the Proceedings World Geothermal Congress 2015.

1563 Zoback, M. D. and Harjes, H.-P. (1997). Injection-induced earthquakes and crustal stress at 9
1564 km depth at the KTB deep drilling site, Germany. *Journal of Geophysical Research: Solid*
1565 *Earth*, 102(B8):18477-18491.

1566 Zoback, M. D., Kohli, A., Das, I., McClure, M. W., et al. (2012). The importance of slow slip
1567 on faults during hydraulic fracturing stimulation of shale gas reservoirs. In *SPE Americas*
1568 *Unconventional Resources Conference*. Society of Petroleum Engineers.

1569 Zoback, M.D., Rummel, F., Jung R., Raleigh C.B. (1977). Laboratory Hydraulic Fracturing
1570 Experiments in Intact and Pre-fractured Rock *Int. J. Rock Mech. Min. Sci. & Geomech.*
1571 *Abstr. Vol. 14*, pp. 49-58.

1572

1573

1574

1575

1576

1577

1578

1579

1580

1581

1582

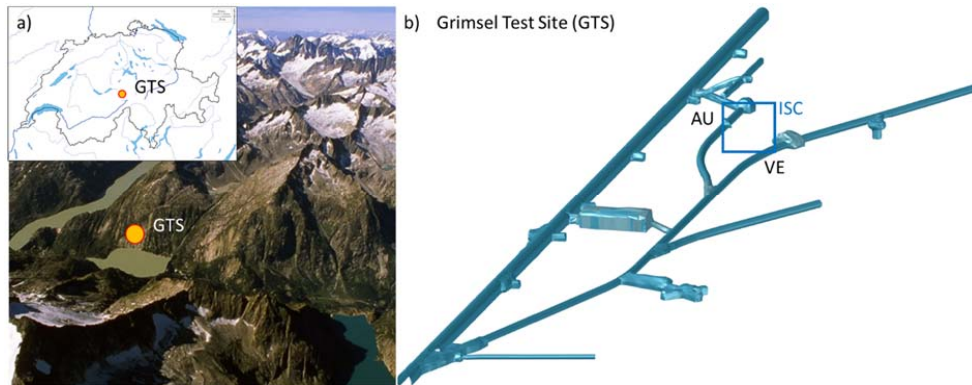
1583

1584



1585

1586



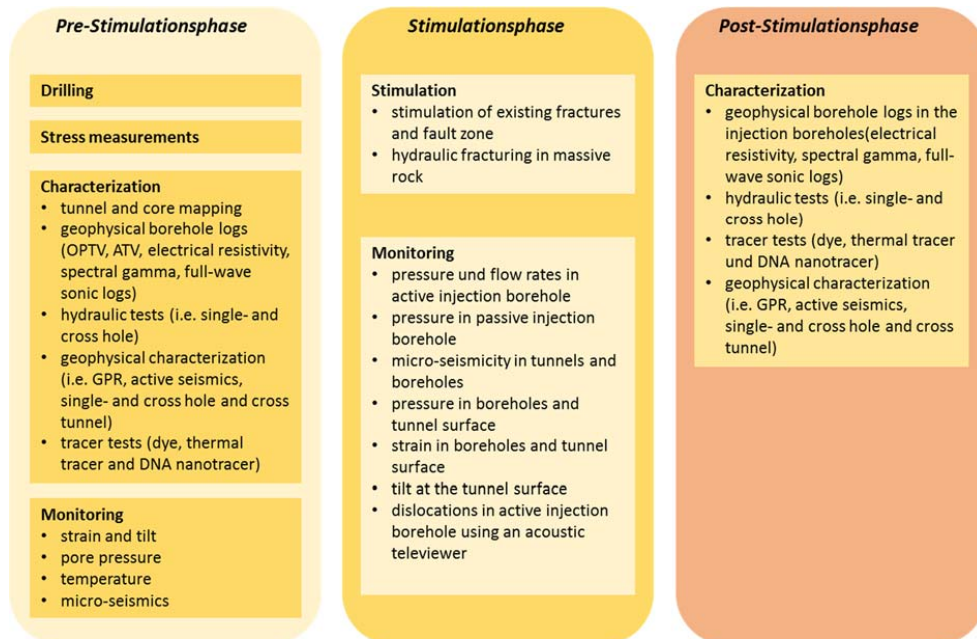
1587

1588 *Figure 1. a) Grimsel Test Site (GTS) is located in the Swiss Alps in the central part of Switzerland. b)*

1589 *The in-situ stimulation and circulation experiment (ISC experiment) is implemented in the southern*

1590 *part of the GTS in a low fracture density granitic rock*

1591

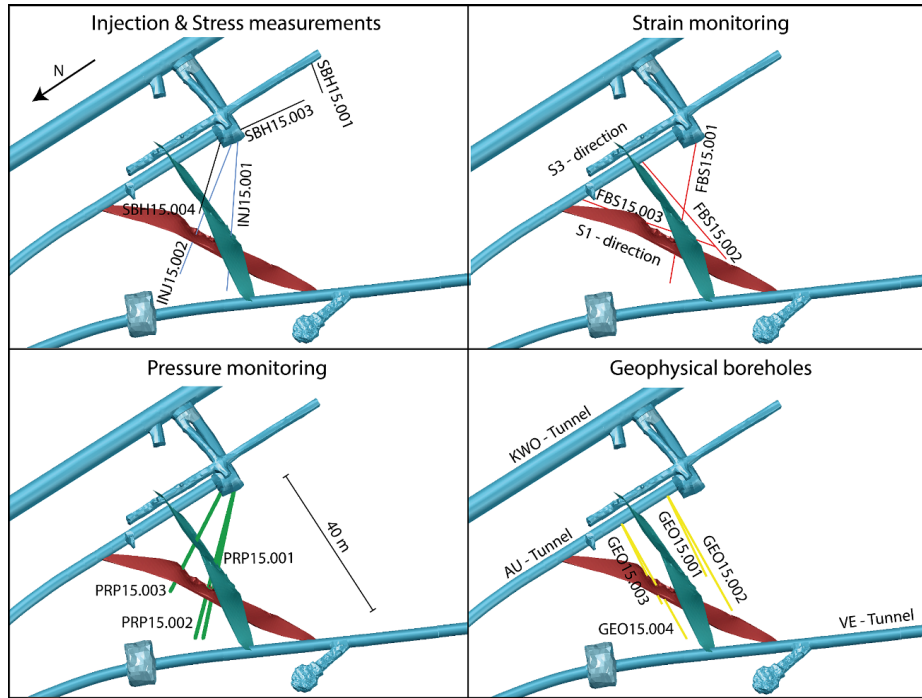


1592

1593 *Figure 2. The three test phases of the ISC experiments with listings of the main activities*

1594 *during each phase.*

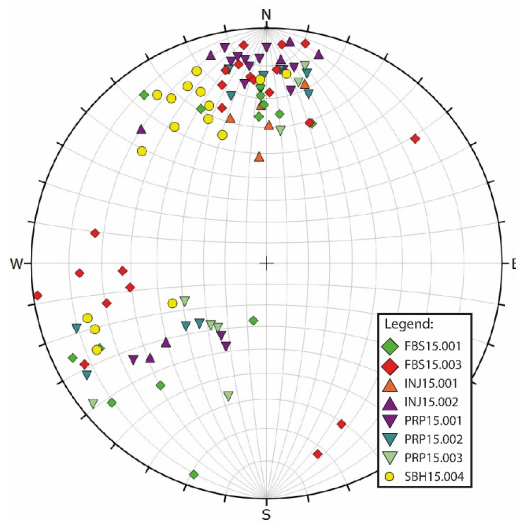
1595



1596

1597 *Figure 3: The 15 boreholes drilled for the ISC experiment (view steeply inclined towards SE).*

1598



1599

1600 *Figure 4. Brittle fractures between meta-basic dykes plotted into the lower hemisphere of a stereonet*
 1601 *plot. The data set is subdivided into the borehole where they were observed.*

1602

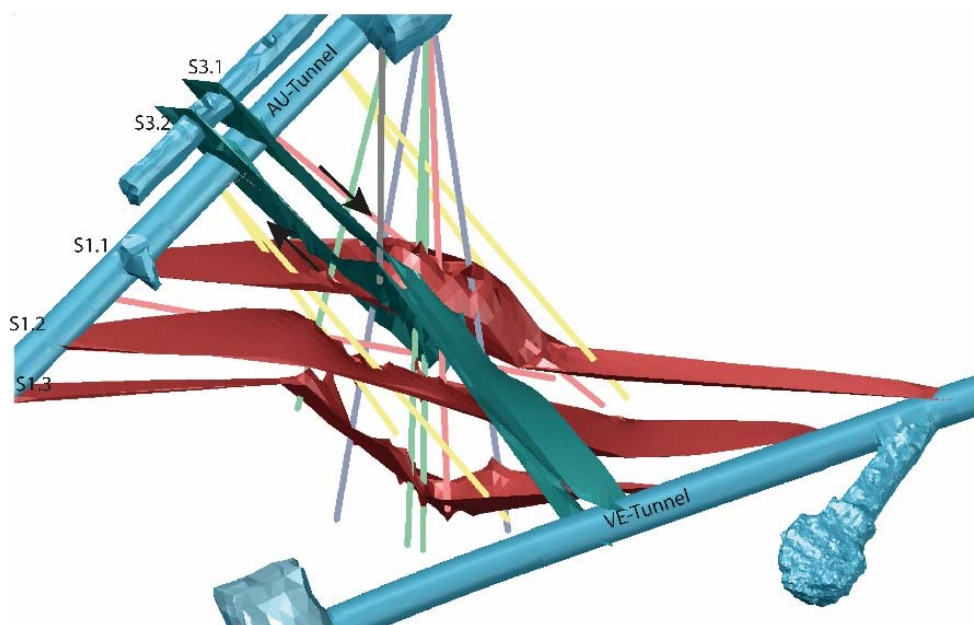


1603

1604

1605

1606

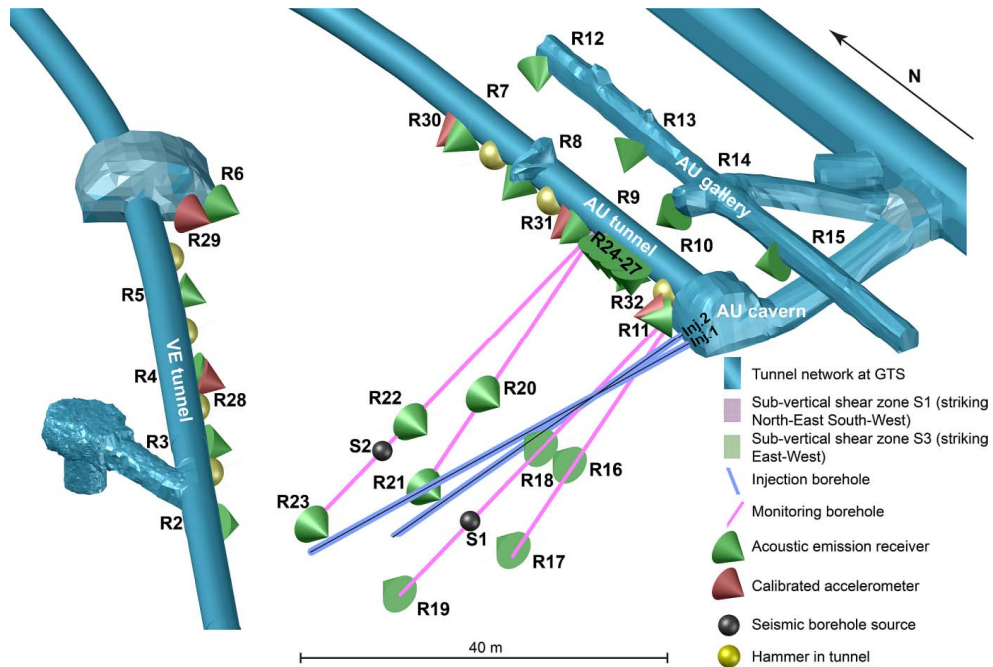


1607

1608 *Figure 5: 3D-Model showing the boreholes drilled towards the rock volume for the in-situ stimulation*
1609 *experiment, S1 (red) and S3 (blue) oriented shear zones as well as the dextral shear sense at the S3*
1610 *shear zones indicated by the black arrows.*

1611

1612



1613

1614 *Figure 6: Outline of seismic monitoring network including hammer sources and borehole*
 1615 *piezosources for active seismic surveys.*

1616

1617

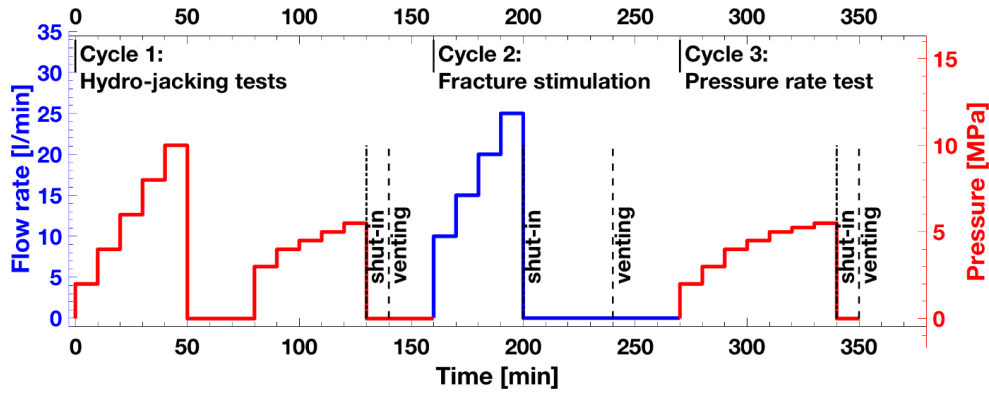
1618

1619

1620

1621

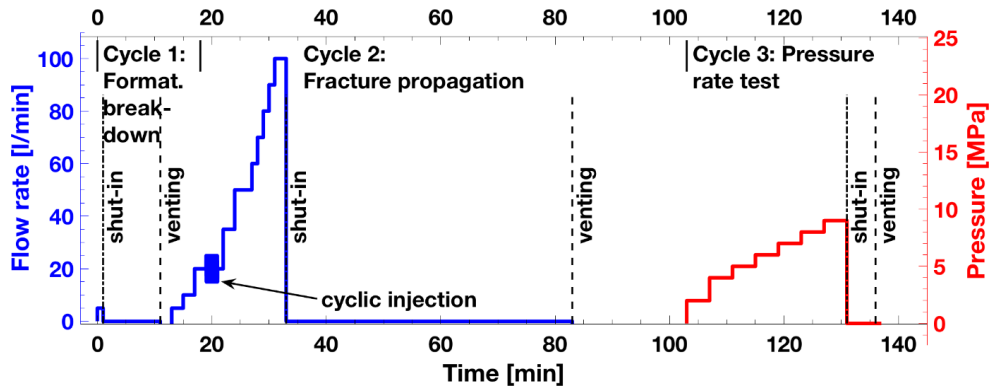
1622



1623

1624

1625 *Figure 7: Planned injection protocol for hydroshearing experiments. Red curves denote*
 1626 *pressure controlled injections. (Cycle 1), blue curves flow rate controlled injections (Cycle 2*
 1627 *and 3). The total volume injected is 1 m³.*



1628

1629 *Figure 8: Planned injection protocol for hydrofracturing experiments. The blue solid curve*
 1630 *denotes flow rate controlled and the red solid curve pressure controlled injection. The red*
 1631 *dashed line respective the blue dashed line are the anticipated pressure respective flow rate*
 1632 *response.*